NASA TN D-1014

TECHNICAL NOTE

D-1014

EXPERIMENTAL SEPARATION STUDIES FOR TWO-DIMENSIONAL WEDGES AND CURVED SURFACES AT MACH NUMBERS OF 4.8 TO 6.2

By James R. Sterrett and James C. Emery

Langley Research Center
Langley Air Force Base, Va.

NATIONAL AERONAUTICS AND SPACE ADMINISTRATION

WASHINGTON

February 1962

NATIONAL AERONAUTICS AND SPACE ADMINISTRATION

TECHNICAL NOTE D-1014

EXPERIMENTAL SEPARATION STUDIES FOR TWO-DIMENSIONAL WEDGES AND CURVED SURFACES AT MACH NUMBERS OF 4.8 TO 6.2

By James R. Sterrett and James C. Emery

SUMMARY

An experimental investigation has been made of the separation phenomena on a flat plate at Mach numbers from 4.8 to approximately 6.2. Emphasis was given to determining the maximum pressure ratio obtainable without separating the turbulent boundary layer for wedges and curved surfaces placed on flat plates. The pressure ratio necessary for separation depends on model shape and Reynolds number if the pressure gradient is of the type produced by wedges and curved surfaces. For example, at a Mach number of 5.8, the maximum pressure ratio without separation for flow over a wedge is approximately 21.8 for conditions near transition and is 11.5 for conditions at the maximum Reynolds number available in these tests. The maximum pressure ratio observed without separation on a curved surface at the same Mach number was approximately 67. When large regions of turbulent separation occur with wedges and curved surfaces, the pressure ratio in the separation region rises to a near constant value for any particular Mach number and is approximately equal to the first peak pressure associated with separation forced by forward-facing steps.

This report gives some insight into the effect of Reynolds number on body forces associated with separation on curved surfaces and wedges. When separation occurs the normal-force coefficient for curved surfaces decreases below the values for nonseparated cases. Normal-force coefficient values for transitional separation are generally less than those for turbulent separation.

INTRODUCTION

Flow separation is a common occurrence in aerodynamics and occurs on any surface where the pressure rise and pressure gradient are sufficiently large. Shock-induced flow separation has been studied extensively at Mach numbers below 4 because of the important influence that separation may have upon the aerodynamics of a configuration. (See refs. 1 to 9.) Much of this previous work has been experimental since

theoretical predictions of separation pressures have been limited because of the simplifying assumptions necessary to solve the flow equations. In general, analytical methods have assumed that the boundary layer follows certain patterns and that several overall average parameters are sufficient to characterize the flow. For example, in references 10 and 11 the Crocco-Lees method utilizes a shape parameter based on the momentum and mass flux within a viscous region. In these theories, it has been necessary to have detailed experimental results to guide in the selection of analytical methods and to check the validity. In much of the previous experimental research, the features of separation have been studied by the investigation of forced separated flow; however, the maximum pressure that could be obtained (on a wedge or curved surface) without separation occurring was much larger than the peak pressure rise in a region where separation had been forced. (See ref. 4.)

In the hypersonic range, relatively little experimental or theoretical work has been attempted on the problem of separation. The purpose of the present program has been to conduct a systematic experimental investigation of boundary-layer separation phenomena at Mach numbers of 4.8 to approximately 6.2. Emphasis has been given to determining the pressure rise necessary to separate a turbulent boundary layer for two-dimensional compression wedges and curved surfaces placed on a two-dimensional flat plate. Also this report gives some characteristics of the flow after separation has occurred. A similar investigation for separation produced by forward-facing steps in the hypersonic range is reported in reference 12. Data of the present paper should aid in the prediction of parameters necessary for separation and will give some insights into body forces associated with separation.

SYMBOLS

C_N normal-force coefficient, $F_N/q_o l$

C_A axial-force coefficient, $F_A/q_o l$

F_A axial force per unit width, calculated by integrating the pressure distribution and assuming a pressure of p_o on rear of surface

F_N normal force per unit width, calculated by integrating the pressure distribution and assuming a pressure of p_o on lower surface

l projected length of wedge or curved surface configuration on axis of plate, measured when β is equal to 15° for wedges or when θ is equal to β for curved surface, in. (see fig. 1)

L	length of plate from leading edge to wedge or curved surface, in.
M	Mach number
p	pressure
q	dynamic pressure
R	radius of curvature
R_e	effective Reynolds number, $\frac{U_o}{\nu_o}\frac{(L - x_{tr})}{12}$
U	streamwise velocity
x	distance measured from leading edge along axis of plate; distances for curved surfaces and wedges are projected distances on this axis taken when β is equal to 15° for wedges or when θ is equal to β for curved surfaces (see fig. 1), in.
y	perpendicular distance from plate, in.
δ	boundary-layer thickness, in.
δ^*	displacement thickness of boundary layer, a Prandtl number of 1 and zero heat transfer being assumed, in.
θ	angle of arc on curved surface (see fig. 1(b))
β	angle of wedge or angle that straight section of curved surface model makes with plate (see fig. 1)
μ	viscosity coefficient
ν	kinematic viscosity, μ/ρ
ρ	density

Subscripts:

o	undisturbed conditions ahead of pressure rise, outer edge of boundary layer
p	first peak conditions for turbulent flow
s	separation point

t total or stagnation conditions

tr end of transitional boundary layer (beginning of fully turbulent boundary layer)

APPARATUS AND TEST METHODS

Wind Tunnel

The test program was conducted in the Langley 20-inch Mach 6 tunnel. This facility operates intermittently from a reservoir at stagnation pressures from 20 to 27 atmospheres with stagnation temperatures up to approximately 600° F. A further description of the tunnel is given in reference 12.

L 1 8 1 2

Models and Supports

Two flat plates were employed, each being designed to provide two-dimensional flow conditions over the areas of interest. The flat-plate portion of the model was 10 inches wide and 1 inch thick with a 10° front wedge that tapered to a cylindrical leading edge of 0.002 of an inch or less. One of the flat plates was 19.30 inches long; the other one was 11.25 inches long. Pressure orifices were located along the chord near the center of the span.

The first basic model consisted of the flat plate and a wedge which was fitted to the downstream end of the flat plate at angles varying from 8° to 35°. A sketch of this model is presented in figure 1(a). A typical designation for one of the wedge models is 11-W-15; this designation identifies the model that has the dimension L of 11.25 inches, the letter W identifies wedge, and 15 identifies the angle of the wedge with respect to the flat plate. The second model was made up of the flat plates and curved surface configurations as shown in figure 1(b). The straight section following the curved portion of the surface was always tangent to the curved surface; however, the total turning angle β of the model could be increased as much as 8° by moving the curved surface configurations relative to the basic flat plate. This condition would result in a slight wedge where the curved surface joined the basic flat model. A typical designation for one of the curved surface configurations is 19-C2028-3.25 and describes a model having a length L of 19.30 inches, C identifies curved surface as opposed to wedge, 20 is the angle θ in degrees, 28 is the angle β in degrees, and the last number is the radius of curvature R of the curved surface. The angle β could be varied from 20° to approximately 48° by using the different configurations of figure 1(b). The support system for each model is the same as that used in reference 12.

Test Methods and Techniques

Variation in Mach number.- The Mach number of the flow along the plate was varied by changing the angle of attack of the plate. This method produced a Mach number change from 4.8 to 6.25 and changed the unit Reynolds number on the plate. The heat necessary to prevent liquefaction was not available for Mach numbers above 6.25.

Pressure measurement.- Static pressures on the model were recorded by photographing a multiple-tube manometer using either butyl phthalate or mercury.

Boundary-layer trips.- The boundary-layer trip consisted of a full-span roughness strip of aluminum oxide grit 1/2 inch wide streamwise and having a maximum height of 0.050 inch. This strip was bonded to the flat plate approximately $1\frac{1}{2}$ inches from the leading edge. The thickness of the plastic bond was approximately one-half the height of the grit.

Boundary-layer measurement.- A total-pressure probe (ref. 12) with a flattened tip was used to survey the boundary layer. The probes were mounted on a 1/4-inch steel tube and could be moved streamwise approximately $10\frac{1}{2}$ inches. The probe position accuracy normal to the plate was ±0.002 inch. Typical examples of fully developed turbulent boundary-layer profiles on the basic flat plate with different effective Reynolds numbers are shown in figure 2. Also shown in this figure is a laminar profile taken on a similar plate from reference 12. (See ref. 12 also for additional velocity profiles.)

Reynolds number.- The Reynolds number for the models at any constant Mach number could be varied only slightly by changing the stagnation pressure because of the small operating pressure range of the tunnel. Therefore, all tests were run at a constant stagnation pressure of 365 pounds per square inch absolute. (This value gave a Reynolds number on the plate of 7.9×10^6 per foot at a Mach number of 5.6.) The Reynolds number was varied by changing the length of the plate ahead of the wedge or curved surface. The roughness strip placed near the leading edge of the plate was used to increase the effective Reynolds number. For purposes of analysis, the effective Reynolds number is defined as the Reynolds number based on the distance from the end of transition to the beginning of the wedge or curved surfaces. Since transition generally occurs over a large distance and is difficult to locate, the concept of a transition point is somewhat ambiguous. In this report, the end of transition was chosen as that region where the shadowgraph showed that the flow had become fully turbulent. This definition of effective Reynolds number has, of course, rather severe limitation inasmuch as it does not describe the past history of the boundary layer which may be important when boundary-layer trips are used.

Optical techniques.- Shadowgraphs and schlieren pictures, as well as velocity profiles, were used to determine the type of boundary layer that existed on the flat plate near the beginning of the curves and wedges. This type of shadowgraph method has been discussed in references 3, 12, and 13. This method utilizes the principle that a laminar density profile deflects the light rays more than a turbulent density profile. Two shadowgraphs which demonstrate this principle are shown in figure 3. The end of the thick white band in these figures indicates that the flow has become fully turbulent. Several schlieren photographs which illustrate the appearance of the boundary layer are shown in figure 4. In general, the physical outline of the boundary layer is more discernible in the schlieren photographs than it is in the shadowgraphs because the second mirror and lens in the schlieren system bring the light rays back to their approximate true position in the flow field. However, it is the lack of this same focusing effect which makes the end of transition more noticeable in shadowgraphs than in the schlieren photographs. The beginning of transition is assumed to occur at the point in the schlieren photograph where the boundary layer suddenly starts to thicken. The end of transition was assumed to occur in the region where the thick white band ends in the shadowgraph.

TYPES OF BOUNDARY-LAYER SEPARATION AND BOUNDARY-LAYER CONDITIONS

One of the predominant variables in separated flow is the location of transition relative to the separation point and the flow reattachment point. This transition location has been discussed in several publications (for example, refs. 3 and 12); however, some of the characteristics are repeated herein for the clarity of this paper. Separated flow can be classified into the following three regimes: pure laminar separation with transition downstream of reattachment, transitional separation with the end of transition between the separation and reattachment points, and turbulent separation with the end of transition upstream of the separation point. Typical pressure distributions for the three types of separation are sketched in figure 5 for separation forced by a forward-facing step. The first peak pressures for turbulent separation are relatively independent of Reynolds number. The two extreme cases for transitional separation are shown in figure 5.

Somewhat similar pressure characteristics for separated supersonic flow over curved surfaces and wedges are given in references 3 and 4 for laminar and turbulent separation. As shown in references 4 and 14, if the flow has not separated, a turbulent boundary layer with low Reynolds numbers can withstand a larger pressure rise without separation

than a turbulent boundary layer with a high Reynolds number. (This condition was observed on wedges and curved surfaces in ref. 4.) Although a generally accepted theoretical explanation does not exist, it seems reasonable to associate these trends partially with the local skin-friction coefficient. (For example, refs. 3 and 7 indicated that the pressure necessary for separation is a function of the skin-friction coefficient.) A sketch showing the coefficient of local skin friction with Reynolds number is shown in figure 6. (See, for example, refs. 15 and 16.) Separation data taken in the transitional region might be expected to vary considerably since the skin-friction coefficient varies markedly.

In general, the following comments regarding the boundary layer for tests of this report were drawn from the shadowgraphs, the schlieren photographs, and the velocity profiles. The laminar boundary layer is relatively stable at hypersonic Mach numbers and a fully developed turbulent boundary layer caused by natural transition does not occur on the 11.25-inch plate for Mach numbers above 4.8. For the smooth 19.3-inch plate, it is questionable whether a fully developed turbulent boundary layer exists for Mach numbers above 6.0. (For a Mach number of 5.8 the schlieren photographs of flow over smooth plates show that transition begins approximately at a Reynolds number of 3.5×10^6 based on distance from leading edge and the shadowgraph shows that transition ends approximately at a Reynolds number of 11×10^6.) A fully developed turbulent boundary layer could be induced on the rear portion of both plates by roughness strips for all Mach numbers under 6.25; however, it is somewhat questionable whether a fully developed turbulent boundary layer existed on the rear portion of the 11.25-inch plate at a Mach number of 6.25. Unless otherwise noted, the data of this report are restricted to fully turbulent boundary-layer data.

RESULTS AND DISCUSSION

The occurrence of separation was very evident from an inspection of the pressure distributions for flow over curved surfaces where the flow changes very suddenly from attached to separated flow. When separation occurred, the pressure distribution always showed a hump in the pressure near the curved surface. This method of determining separations has been used in reference 4 and elsewhere. A typical example is shown in figure 7(a) which shows the pressure distribution with and without separation for the same curved surface. The boundary layer is turbulent for both cases. However, the effective Reynolds number has been increased by placing roughness on the front of the plate for the separated case. Whether separation occurs for a wedge is not as evident as for the curved surface. Figure 7(b) shows the pressure distribution over a 28° wedge with and without separation. Conditions are again such that

separation occurs with roughness on the plate as is shown by the inflection point (or hump) in the pressure distribution. This hump does not appear when the flow remains attached to the surface.

Flow Over Wedges

The figures presenting the test results for the flow over wedges are as follows:

	Figure
Pressure distributions with an increase in wedge angles for various effective Reynolds numbers	8
Maximum wedge angle without separation at various Mach numbers	9(a)
Maximum pressure ratio without separation at various Mach numbers	9(b)
Parameters as a function of effective Reynolds number	10
Normal- and axial-force coefficients for different wedge angles at various effective Reynolds numbers	11
Comparison of pressure distributions over equal wedge angles at different Reynolds numbers	12 and 13

The maximum pressure ratio for attached flow over wedges at a constant Mach number was obtained by comparing pressure distributions over wedges whose angle had been changed by discrete increments for the same boundary-layer conditions. Pressure distributions which illustrate the occurrence of separation with an increase of wedge angle for different effective Reynolds numbers at a Mach number of 5.8 are shown in figure 8. In figure 8(a), when the wedge angle is increased to an angle of $25^{\circ}45'$, a small amount of separation exists as is shown by the slight hump in the pressure distribution. As the wedge angle is increased further, the pressure hump moves forward; this movement indicates that the beginning of separation has moved further forward on the plate. It is interesting to note the first peak pressure and the pressure at separation produced by forward-facing steps as given in reference 12 for this Mach number. They are approximately 4.2 and 3.0, respectively, and are shown in figure 8(a) for comparison with the 33° wedge which has a large region of separation. In figure 8(b), the effective Reynolds number has been decreased from that of figure 8(a) by placing the wedges on the 11.25-inch plate with roughness. When the wedge angle is increased to 28°, a small amount of separation

exists. A comparison of this pressure distribution with the distribution of a similar wedge in figure 8(a) shows that, although both have separated flow, the separation region is much larger in figure 8(a) where the effective Reynolds number is the largest. In figure 8(c) where the Reynolds number has been decreased by using a smooth plate before the wedge, much higher wedge angles are attainable without separation occurring. It is somewhat difficult to tell exactly from the data of figure 8(c) when separation occurs since the increase of pressure is felt much before the actual start of the wedge. However, the first significant hump in the pressure distribution is not seen until the wedge angle becomes approximately 34°. As pointed out in references 4 and 17, it is possible that a small separated region is always present at the beginning of a wedge. However, the important factor here is that a sizeable region of separated flow is always accompanied by a hump in the pressure distribution, and that the appearance of a small pressure hump signals the beginning of a change in the boundary layer which subsequently grows into a large-scale separation as the wedge angle is increased.

L
1
8
1
2

The maximum pressure ratio and wedge angle for attached flow over wedges at various effective Reynolds numbers are shown in figure 9. The faired data of figure 9(b) has been replotted in figure 10(b) as a function of the effective Reynolds number. The approximate effective Reynolds numbers for the different plates as a function of Mach number are given in figure 10(a). As can be seen from figures 9 and 10, the peak pressure rise and wedge angle necessary to force separation depend significantly upon Reynolds number. The maximum pressure ratio and wedge angle allowable without separation occurring increases as the effective Reynolds number (for a constant Mach number) is decreased. For example, at a Mach number of 5.8, the flow can turn approximately 24° without separation when the flow has the maximum Reynolds number available for these tests. The flow for model 19W without roughness can be turned approximately 31° without separation occurring; this condition results in a pressure ratio of approximately 21.8. Data points for the plates without roughness are not shown at the higher Mach numbers since transitional separation occurred under these conditions. Also shown in figure 9 are similar data taken from reference 4 at lower Mach numbers. The present data agree reasonably well with these lower Mach number data. In reference 4 it was shown that the influence of a change in Reynolds number on pressure ratio necessary to produce separation was less in the high Reynolds number range of turbulent flow. There is indication of this effect from the present data of figure 10(b) since the pressure ratios necessary for separation increase rapidly as the effective Reynolds number approaches transitional conditions. Figure 10(b) also indicates that, if the effective Reynolds number remains constant, increasing the Mach number would increase the pressure ratio that the flow can undergo without separation occurring.

The variation of the extent of boundary-layer separation can obviously affect the normal and axial forces on a body. Figure 11 shows a comparison of the normal- and axial-force coefficients for different wedge angles with different effective Reynolds numbers at several Mach numbers. Most of the data points in this figure are for turbulent boundary layers; however, a few points are included which have transitional separation. The experimental normal- and axial-force coefficients (C_N and C_A, respectively) were obtained by mechanically integrating the pressure distributions. The theoretical inviscid normal- and axial-force coefficients were obtained by assuming oblique shock values. The experimental data of figure 11 are always less than the theoretical data. The experimental data can vary when the effective Reynolds number is changed for turbulent flow before a wedge. In general, for a turbulent boundary layer, these coefficients decrease as the effective Reynolds number (of any constant Mach number) is increased, the greatest decrease occurring for the 19.3-inch plate with roughness. At a Mach number of 6.2, transitional separation occurs for the smooth 19.3-inch plate at the higher wedge angles, and the coefficients decrease to their lowest values for that Mach number. No sharp demarcation of the coefficients occurs between separated and nonseparated flow.

L 1 8 1 2

An inspection of the pressure distributions in figures 12 and 13 for flow over approximately equal wedge angles gives a further insight into why the force coefficients can vary with a change in effective Reynolds number. For example, in figure 12(c), it is seen that, when the flow remains attached for model 19W without roughness, the pressure rises to a value greater than the theoretical shock value for a 28° wedge. When the flow passes over a similar wedge angle placed on model 11W with roughness, a very small amount of separation exists, and the pressure rises more slowly to a value slightly above the theoretical shock value. For model 19W with roughness, a larger region of separation exists, and the pressure does not rise quite to the theoretical shock value. This effect is apparently partially due to the fact that the turning of the flow has been delayed and the flow has not turned an amount equal to the wedge angle at the end of the wedge. For model 11W without separation, the pressure rises rapidly near the beginning of the wedge and rises to a value approximately equal to the theoretical value. The forces on the model, of course, depend not only on the maximum pressure ratio, but upon the pressure rise gradient and the location of the initial pressure rise.

A similar comparison for turbulent separated flow and attached flow at a higher Mach number is shown in figure 13. Also shown in this figure is an example of transitional separation when model 19W without roughness was used. The beginning of the pressure rise moved very far forward and the peak pressure is much below the theoretical shock value. Apparently, the flow at the end of the wedge has turned much less than the actual wedge angle.

Curved Surfaces

Experimental studies of flow over curved surfaces at supersonic Mach numbers (ref. 4) have established that making a surface curved delays separation. Reference 4 also shows that test conditions at which separation first occurs is often different from the conditions at which separation first disappears. Figures 14 and 15 present pressure distributions which illustrate this separation hysteresis effect at hypersonic speeds. The same Mach number was obtained by changing the plate angle so that in one case the Mach number was increased while going from attached flow conditions; and, in the other case the Mach number was decreased while going from conditions where separation had occurred. For a Mach number of 4.8 (fig. 14(a)) the flow was attached whether the Mach number was increased or decreased. At a Mach number of 4.95 (fig. 14(b)), the flow was attached when increasing the Mach number and separated when decreasing the Mach number. This condition continued until at a Mach number of 5.8 the flow was separated regardless of whether the Mach number was increased or decreased.

Examples of separation occurring with contrary Mach number trends are shown in figure 15. At Mach numbers below 4.8 for these test conditions, the flow separates and remains separated when the Mach number is increased to 4.8. If the Mach number of 4.8 is obtained by lowering the Mach number from attached conditions, the flow remains attached. The important factor to be noted from figures 14 and 15 is that, if separation has already occurred, the flow may remain separated for conditions which otherwise would give attached flow.

The maximum conditions for attached flow over curved surfaces at a constant Mach number were obtained by comparing pressure distributions over curved surfaces whose surface angle had been changed by discrete increments for the same boundary-layer conditions. Pressure distributions illustrating the occurrence of separation with an increase of surface angle for different effective Reynolds number at a Mach number of 5.8 for models with a 3.25- and 2.00-inch radius are shown in figure 16. (The effective Reynolds numbers for the basic plates are shown in fig. 10(a).) These data were taken when changing from the attached condition toward the separated condition unless separation occurred for all conditions. In figure 16(a) when the surface angle was increased to an angle of 33°37' or greater, separation occurred as is shown by the hump in the pressure distributions. As the surface angle is increased, the separated region moved further forward on the plate. The first peak pressure and pressure at separation produced by the forward-facing steps of reference 12 for this Mach number for a fully turbulent boundary layer are also shown in figure 16(a). As with wedges, when large regions of turbulent separation occur, the peak pressure in the separated region was approximately the same as that produced by forward-facing steps with a turbulent boundary layer.

In figure 16(b), the effective Reynolds number has been decreased from that of figure 16(a) by using the 11.25-inch plate with roughness. The model surface angle can now be increased to over 40° without separation occurring. These same results are shown by the schlieren photographs of figure 17 which are for the conditions shown in figure 16(b). The effective Reynolds number has been decreased still further in figure 16(c) by using the smooth 19.3-inch plate. It is necessary to increase the surface turning angle to over 46°, which is greater than the theoretical wedge shock-detachment angle before separation occurs. The beginning of separation moves very far forward and transitional separation results. Similar pressure distributions which show the same trends for the models with a 2.00-inch radius are shown in figures 16(d) and 16(e).

The maximum surface angle for attached flow and the angle where separation first was noted for various effective Reynolds numbers is shown in figure 18. Figure 19 shows the maximum pressure ratios for attached flow. The maximum pressure ratios (fig. 19(a)) for the 19.3-inch plate without roughness were observed with the 44° turning model. The pressure ratios observed with the maximum turning of 46° for this configuration are given by the solid circles of figure 19(a). Data for these plots were obtained from pressure distributions similar to those of figure 16. Data for the smooth 19.3-inch plate with Mach numbers above 6 are not given in these plots since transitional separation occurred. A comparison of the data in figure 18(a) with that of figure 18(b) shows that, if all other conditions remain constant, the flow can be turned through a larger angle without separation for the 3.25-inch radius model than for the 2.00-inch radius model. These figures also show that the maximum turning angle without separation depends partially upon the Reynolds number. Reynolds number effects on the maximum turning angle apparently become less significant as the radius of curvature is increased. The maximum turning angles without separation tend to decrease at the higher Mach numbers for the maximum Reynolds numbers. The exact reason for this is not known; however, it should be remembered that these data are grouped together for the same actual radius of curvature and not for some radius based on boundary-layer parameters.

A comparison of some calculated and experimental pressure distributions over curved surfaces with attached flow is given in figure 20. The surface slopes of the two models in the figure are identical up to 34°; however, one model continues the turning to 44°. The dashed lines for oblique shock theory of figure 20 were obtained by considering the surface as composed of flat elements of 2° of arc and ignoring reflected waves. In general, the experimental pressures are less than that calculated by the incremental oblique shock method and are greater than that calculated by Newtonian theory.

The maximum pressure rise for the curved surfaces without separation might be expected to fall between the near isentropic values of the small-increment oblique shocks and the oblique shock values for a wedge angle equal to the total surface turning. When the total turning is less than the theoretical wedge shock detachment angle, the maximum pressure on the surface with nonseparated flow is slightly greater than the oblique shock value for an angle equal to the total surface turning. (See figs. 16 and 20.) It is possible for the maximum local pressure ratio to obtain a very high value when the surface turning angle is greater than the theoretical wedge shock detachment angle. A typical example of this effect is shown in figure 20 for the 44° turning surface. Apparently, the flow passes through a strong shock with subsonic flow behind the shock; the flow then rapidly expands downstream of the shock. Additional evidence of these phenomena can be observed in the schlieren photograph of figure 15(c) which indicates a strong shock located in the vicinity of the curved surface.

L
1
8
1
2

The normal-force coefficient generated by the curved plate and the effect of separation upon C_N is shown in figure 21. For the 46° surface turning case (fig. 21(a)) both separated and attached data were obtained on the smooth plate by the hysteresis method previously discussed and an increase in effective Reynolds number was obtained by the addition of roughness near the leading edge of the plate. It can be seen that a change in effective Reynolds number for a constant Mach number has little effect upon C_N provided the flow remains attached. When separation does occur, the normal-force coefficient decreases in all cases. As the separation region decreases, C_N approaches the value for attached flow; for example, in figure 21(b), C_N has only been reduced approximately 9 percent by separation at a Mach number of 5.2. When transitional separation occurs, C_N is generally decreased more than for turbulent separation as is shown by the smooth-plate data at the higher Mach number. (See fig. 21.) One exception to this is shown by the smooth-plate data of figure 21(a) at a Mach number of 5.45. It is in this region that the flow changes from turbulent to transitional separation and all data for the smooth plate at this Mach number and above is of the transitional separation type. An inspection of the pressure distributions in figure 22 gives a further insight into C_N variation with a change in effective Reynolds number for a model with a large region of separation. If the beginning of separation remains in a region where the boundary layer is fully turbulent (as in figs. 22(a) and 22(c)), the pressure ratio in the separation region rises to a constant plateau value approximately equal to that caused by a forward-facing step and the pressure distributions remain approximately constant with a change in Reynolds number. For transitional separations (see smooth-plate data of figs. 22(b) and 22(d)), the pressures in the separation regions are much lower than those for turbulent separation.

Schlieren photographs for the conditions given in figure 22(c) and 22(d) are shown in figure 23. These photographs indicate that the position of the separation point relative to the wedge remains approximately constant for a turbulent boundary layer with a change in effective Reynolds number for a constant Mach number but moves a considerable distance forward when transitional separation occurs. It is interesting to compare the pressure distributions with separated flow over a model for the 19.3-inch plate with roughness at several different Mach numbers. (Compare fig. 22(a) with fig. 22(b) and fig. 22(c) with fig. 22(d).) The beginning of separation moves forward with an increase in Mach number if the beginning of separation occurs in a region where the boundary layer is fully turbulent. Also sketched in those figures are the calculated pressure rise and reattachment points for turbulent separation if it is assumed that the flow separates at the beginning of the pressure rise and has a constant flow deflection angle equal to that calculated from the pressure-ratio data for the forward-facing steps of reference 12.

L 1 8 1 2

A Comparison of Pressure Ratios Associated With Separation

Two-dimensional separation criteria for turbulent boundary layers are summarized in figure 24. The trends of the present data for the curved surfaces and wedges agree very well with the data of reference 4 which has been included in figure 24. At the lower Mach numbers, the maximum pressure ratios obtained without separation are of the same magnitude as the first peak pressures of separation forced by forward-facing steps. However, as the Mach number is increased, the maximum pressure ratio obtained without separation is in all cases much larger than the pressure ratios associated with forced separation. (It has already been shown that, when large regions of turbulent separation occur with curved surfaces and wedges, the pressure ratio in the separation region rises to a value approximately equal to that for forward-facing steps. This is also true of the maximum pressure ratios associated with the jet-produced separation of ref. 18.) At the higher Mach numbers, the maximum pressure ratios obtainable without separation become very dependent upon shape and Reynolds number. For example, at a Mach number of 5.8, the maximum pressure ratio without separation for wedges is 21.8 for conditions near transition and 11.5 for conditions with the maximum Reynolds number available in these tests. The maximum pressure ratio at this same Mach number near transition conditions is approximately 67 for a curved surface with a 3.25-inch radius. A region which shows the approximate magnitude of the plateau and separation pressures for laminar separation over forward-facing steps is shown in figure 24. There are some experimental data for curved surfaces and wedges (not given in fig. 24) which show that, if the boundary layer is transitional, the pressure ratio necessary for separation is less than that for fully turbulent flow. However, the boundary-layer parameters are

changing very rapidly in the transitional region, and it is believed that a generalized conclusion cannot be drawn from the small amount of existing data.

CONCLUDING REMARKS

An experimental investigation has been made of the separation phenomena on a flat plate at Mach numbers from 4.8 to approximately 6.2. Emphasis was given to determining the maximum pressure ratio obtainable on wedges and curved surfaces without separating the turbulent boundary layer. The maximum pressure ratios obtained without separation are in all cases larger than pressures associated with forced separations. The pressure ratio necessary for separation depends on shape and Reynolds number if the pressure gradient is of the type produced by wedges and curved surfaces. Curved surfaces can withstand larger pressure ratios without separating than wedges. The maximum pressure ratio without separation obtained in the present tests at a Mach number of 5.8 was approximately 67 for a curved surface with a 3.25-inch radius near transitional conditions. With all other conditions remaining constant, the flow was turned through a larger angle without separation for a surface with a 3.25-inch radius than for a surface with a 2.00-inch radius. When the pressure gradient is relatively weak as with curved surfaces, conditions at which separation first occurs may be different than conditions at which separation first disappears. The data indicate that, if the effective Reynolds number remains constant, increasing the Mach number increases the pressure ratio that the flow can undergo without separation occurring for wedges.

A change in the effective Reynolds number has little effect on the normal-force coefficient for the curved surfaces tested as long as the flow remains attached. When separation occurs, the normal-force coefficient C_N decreases in all cases. At a Mach number of 5.8, C_N for a 46° curved surface was 0.41 with turbulent separation and 0.78 with attached flow. The data indicate that C_N values for transitional separation are generally less than those for turbulent separation. The data also show that a change in the effective Reynolds number can vary the body forces on these wedges regardless of whether the flow is attached or separated for turbulent flow. When large regions of turbulent separation occur with wedges and curved surfaces, the pressure ratio in the separation region for any particular Mach number rises to a near constant value approximately equal to the first peak pressure associated with separation forced by forward-facing steps. In large regions of turbulent separation, the pressure distribution remains

approximately constant with a change in Reynolds number and results in approximately constant forces for the same model.

Langley Research Center,
National Aeronautics and Space Administration,
Langley Air Force Base, Va., November 6, 1961.

1. Liepmann, Hans Wolfgang: The Interaction Between Bounday Layer and Shock Waves in Transonic Flow. Jour. Aero. Sci., vol. 13, no. 12, Dec. 1946, pp. 623-638.

2. Ackeret, J., Feldman, F., and Rott, N.: Investigations of Compression Shocks and Boundary Layers in Gases Moving at High Speed. NACA TM 1113, 1947.

3. Chapman, Dean R., Kuehn, Donald M., and Larson, Howard K.: Investigation of Separated Flows in Supersonic and Subsonic Streams With Emphasis on the Effect of Transition. NACA Rep. 1356, 1958. (Supersedes NACA TN 3869.)

4. Kuehn, Donald M.: Experimental Investigation of the Pressure Rise Required for the Incipient Separation of Turbulent Boundary Layers in Two-Dimensional Supersonic Flow. NASA MEMO 1-21-59A, 1959.

5. Bogdonoff, S. M., and Kepler, C. E.: Separation of a Supersonic Turbulent Boundary Layer. Jour. Aero. Sci., vol. 22, no. 6, June 1955, pp. 414-424, 430.

6. Love, Eugene S.: Pressure Rise Associated With Shock-Induced Boundary-Layer Separation. NACA TN 3601, 1955.

7. Lange, Roy H.: Present Status of Information Relative to the Prediction of Shock-Induced Boundary-Layer Separation. NACA TN 3065, 1954.

8. Gadd, G. E.: A Theoretical Investigation of Laminar Separation in Supersonic Flow. Jour. Aero. Sci., vol. 24, no. 10, Oct. 1957, pp. 759-771.

9. Hakkinen, R. J., Greber, I., Trilling, L., and Abarbanel, S. S.: The Interaction of an Oblique Shock Wave With a Laminar Boundary Layer. NASA MEMO 2-18-59W, 1959.

10. Crocco, L.: Considerations on the Shock—Boundary-Layer Interactions. Proc. Conf. on High-Speed Aeronautics, Antonio Ferri, Nicholas J. Hoff, and Paul A. Libbey, eds., Polytechnic Inst. of Brooklyn, c.1955.

11. Glick, Herbert S.: Modified Crocco-Lees Mixing Theory for Supersonic Separated and Reattaching Flows. GALCIT MEMO No. 53 (Contract No. DA-04-495-Ord-1960), May 2, 1960.

12. Sterrett, James R., and Emery, James C.: Extension of Boundary-Layer Separation Criteria to a Mach Number of 6.5 by Utilizing Flat Plates With Forward-Facing Steps. NASA TN D-618, 1960.

13. Pearcey, H.H.: The Indications of Boundary-Layer Transition on Aerofoils in the N.P.L. 20 in. × 8 in. High Speed Wind Tunnel. C.P. No. 10, British A.R.C., 1950.

14. Gadd, G. E., Holder, D. W., and Regan, J. D.: An Experimental Investigation of the Interaction Between Shock Waves and Boundary Layers. Proc. Roy. Soc. (London), ser. A, vol. 226, no. 1165, Nov. 9, 1954, pp. 227-253.

15. Coles, Donald: Measurements in the Boundary Layer on a Smooth Flat Plate in Supersonic Flow. III. Measurements in a Flat-Plate Boundary Layer at the Jet Propulsion Laboratory. Rep. No. 20-71 (Contract No. DA-04-495-Ord 180), Jet Propulsion Lab., C.I.T., June 1, 1953.

16. Matting, Fred W., Chapman, Dean R., Nyholm, Jack R., and Thomas, Andrew G.: Turbulent Skin Friction at High Mach Numbers and Reynolds Numbers in Air and Helium. NASA TR R-82, 1961.

17. Hammitt, Andrew G., and Hight, Sylvester: Scale Effects in Turbulent Shock Wave Boundary Layer Interactions. Proc. Sixth Annual Conf. on Fluid Mechanics, Univ. of Texas, Sept. 1959, pp. 362-382.

18. Romeo, David J., and Sterrett, James R.: Aerodynamic Interaction Effects Ahead of a Sonic Jet Exhausting Perpendicularly From a Flat Plate into a Mach Number 6 Free Stream. NASA TN D-743, 1961.

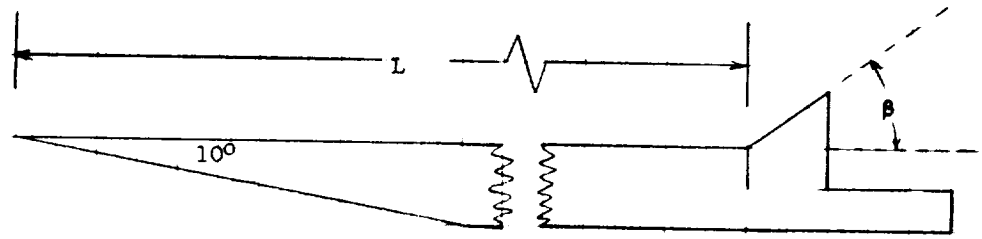

(a) Wedge model.

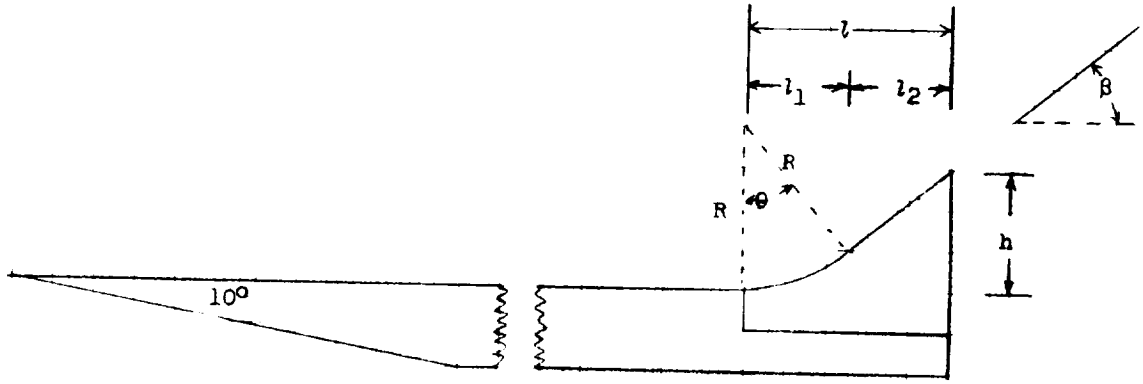

(b) Curved surface model.

R	θ, deg	l_1	l_2	h
3.25	20	1.112	1.388	0.510
3.25	30	1.625	1.075	.870
3.25	40	2.089	.911	1.340
2.00	20	.684	1.816	.600
2.00	30	1.000	1.370	.870
2.00	40	1.286	1.264	1.340

Figure 1.- Model configurations and dimensions.

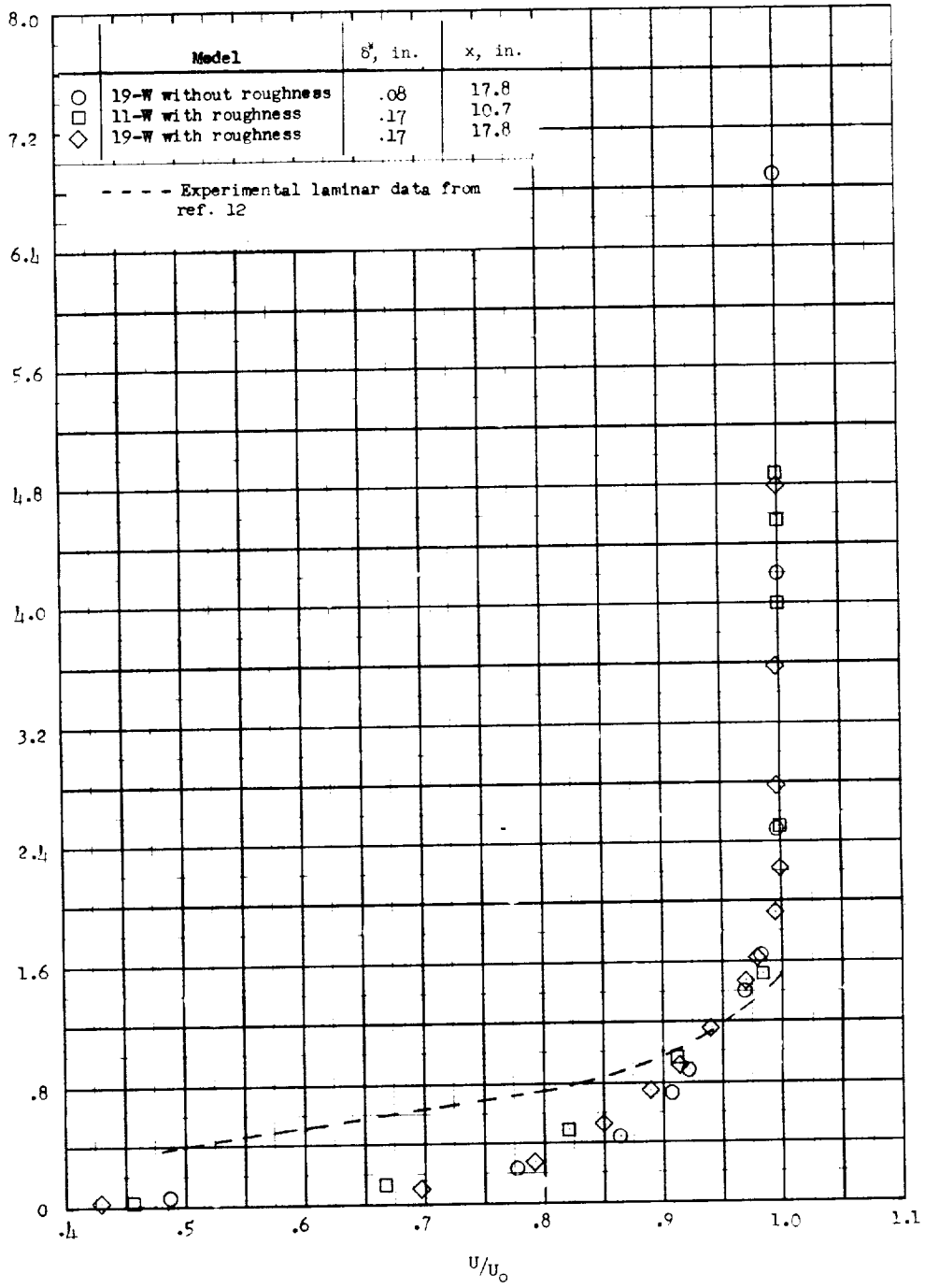

Figure 2.- Typical boundary-layer velocity profiles on the basic flat plate with different effective Reynolds numbers. $M_o = 5.6$; $p_t = 365$ lb/sq in. abs.

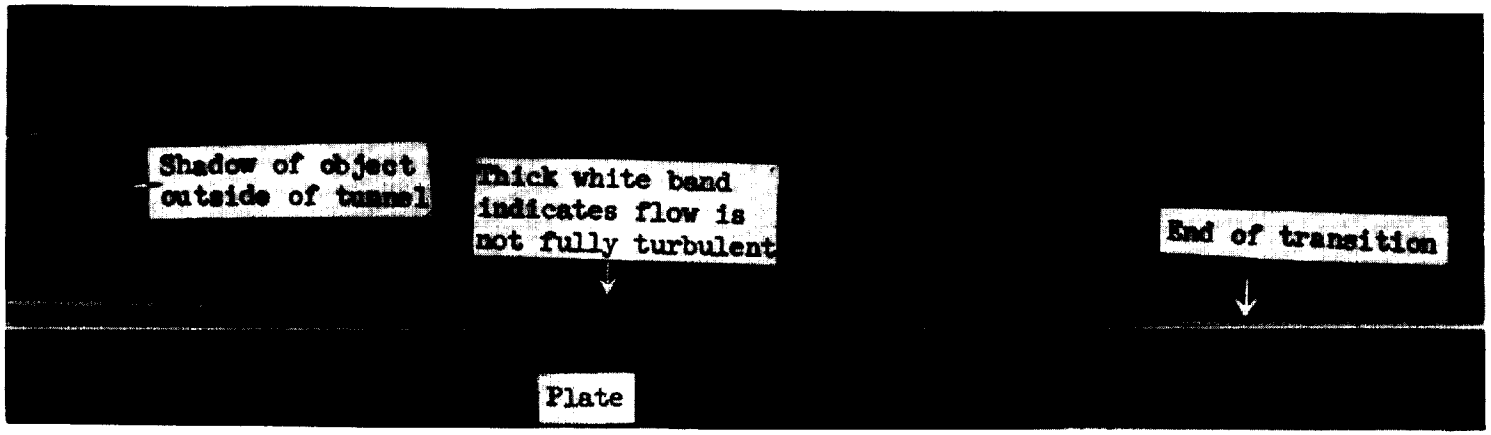

(a) Natural transition on plate. $M_o = 4.8$.

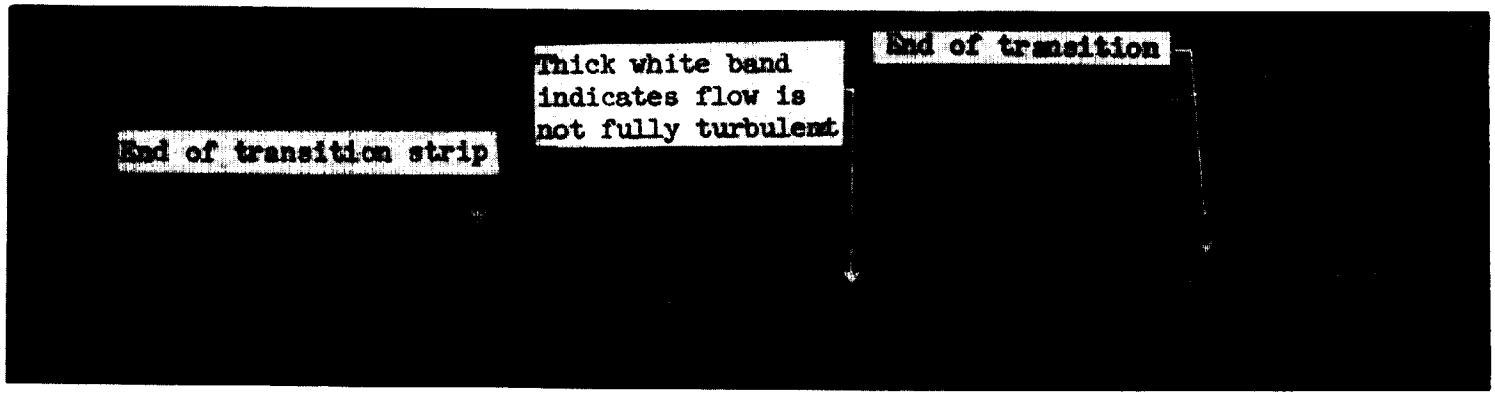

(b) Turbulent boundary layer after trip. $M_o = 5.8$. L-60-5531.1

Figure 3.- Illustration of shadowgraph method for determining type of boundary-layer flow.

(a) Natural transition on a smooth plate. Model 11-C3036-2.00; $M_o = 4.8$.

(b) Natural transition on smooth plate. Model 11-W-28; $M_o = 5.8$.

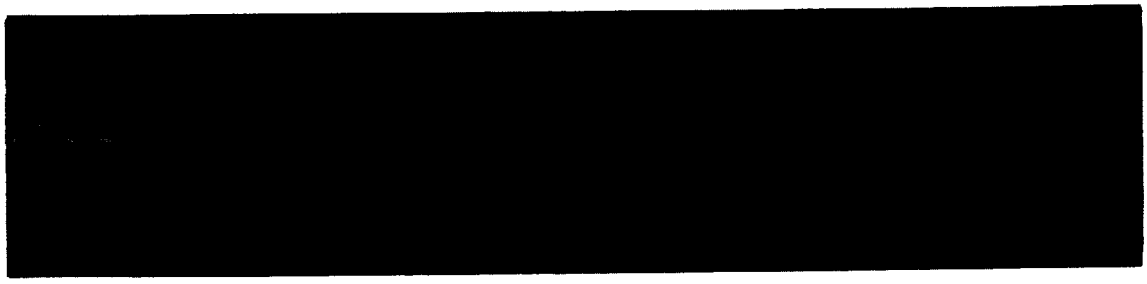

L-61-7733

(c) Forced transition with trip on plate. Model 11-W-8; $M_o = 5.8$.

Figure 4.- Appearance of boundary layer in schlieren photographs.

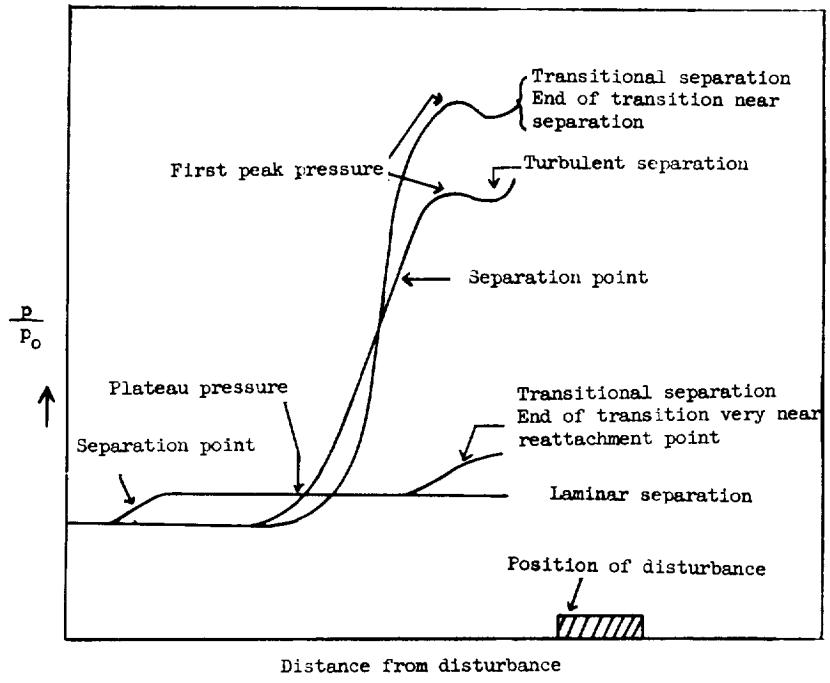

Figure 5.- Pressure distributions for different separation regimes for a forward-facing step.

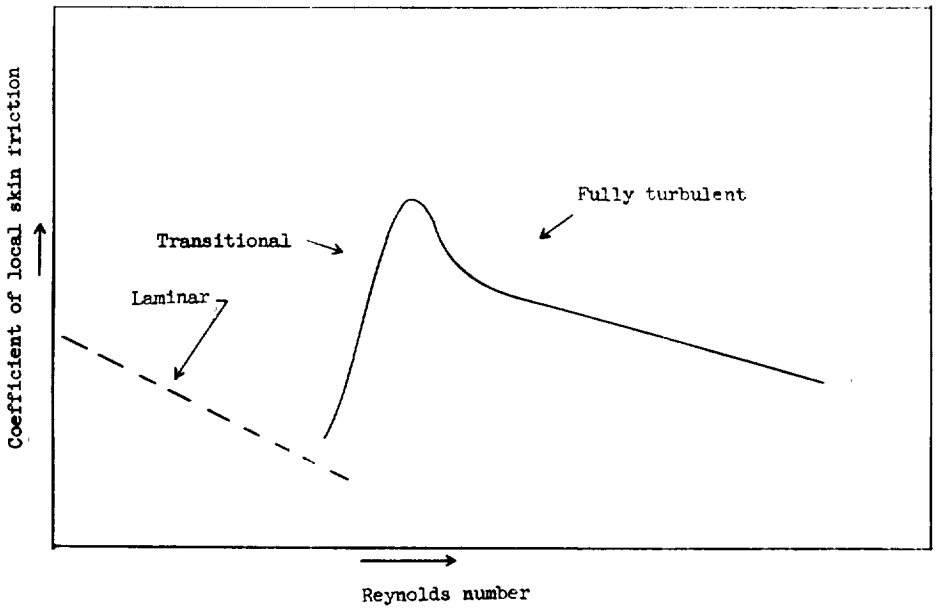

Figure 6.- Sketch showing variation of local skin friction with Reynolds number based on distances from leading edge.

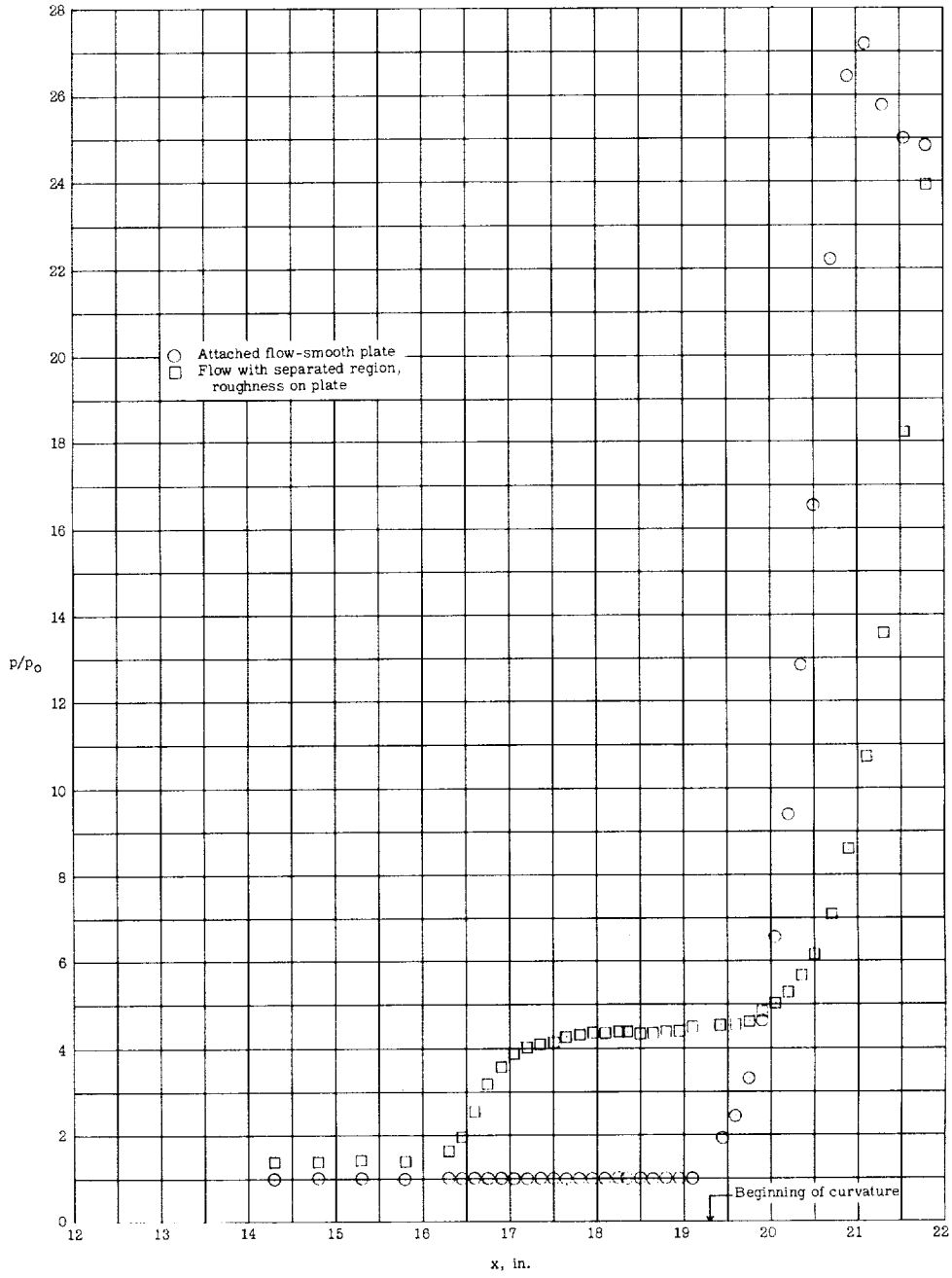

(a) Flow over curved surfaces. Model 19-C3038-3.25.

Figure 7.- Typical examples of the pressure distribution with and without separated flow for models on 19.3-inch plate. p_t = 365 lb/sq in. abs; M_o = 5.8.

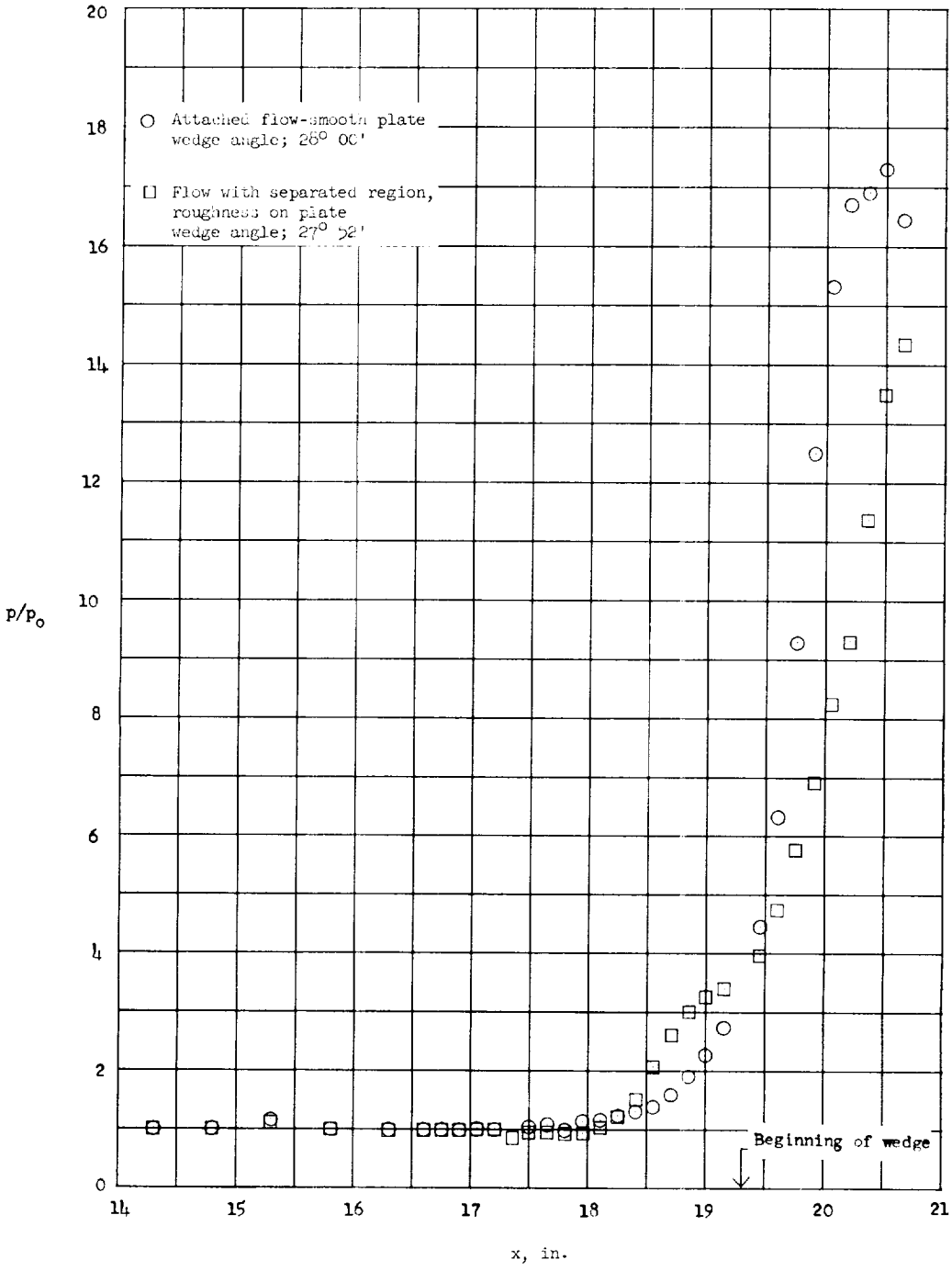

(b) Flow over wedges on 19.30-inch plate.

Figure 7.- Concluded.

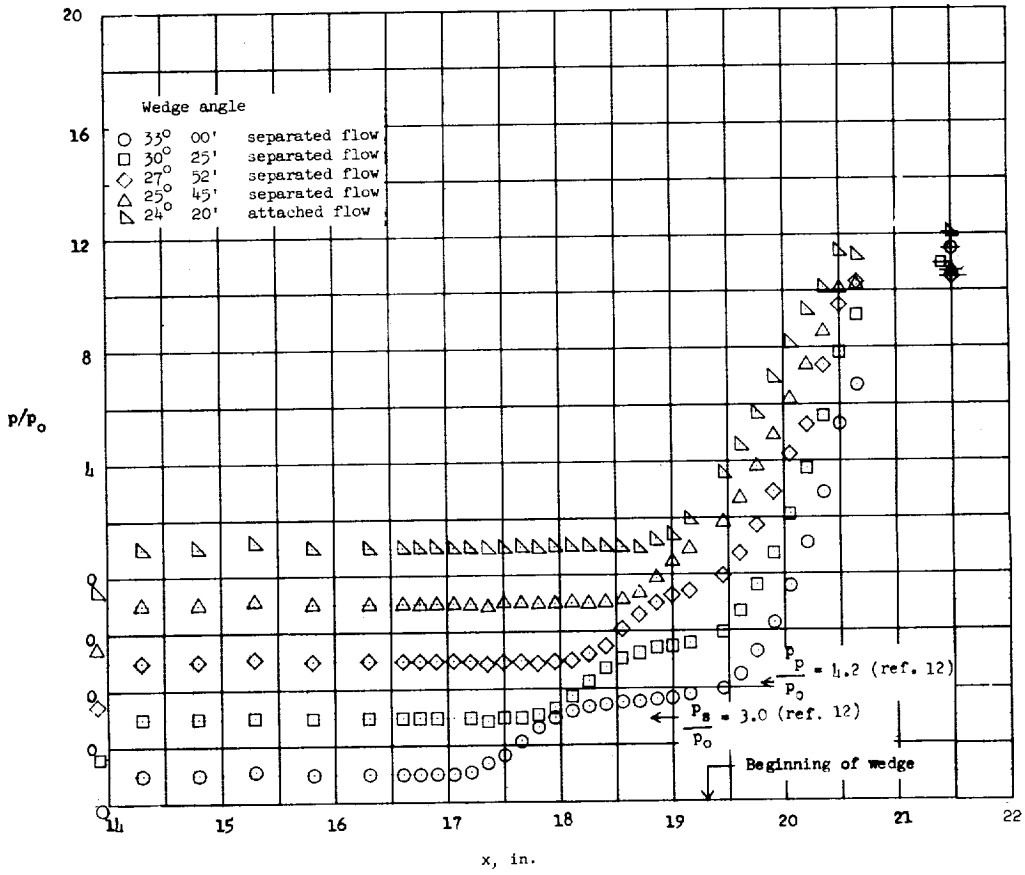

(a) Model 19-W with roughness.

Figure 8.- Pressure distributions illustrating the occurrence of separation with an increase of wedge angle for different effective Reynolds numbers. $M_0 = 5.8$; $p_t = 365$ lb/sq in. abs. Bars through symbols indicate theoretical oblique shock pressures.

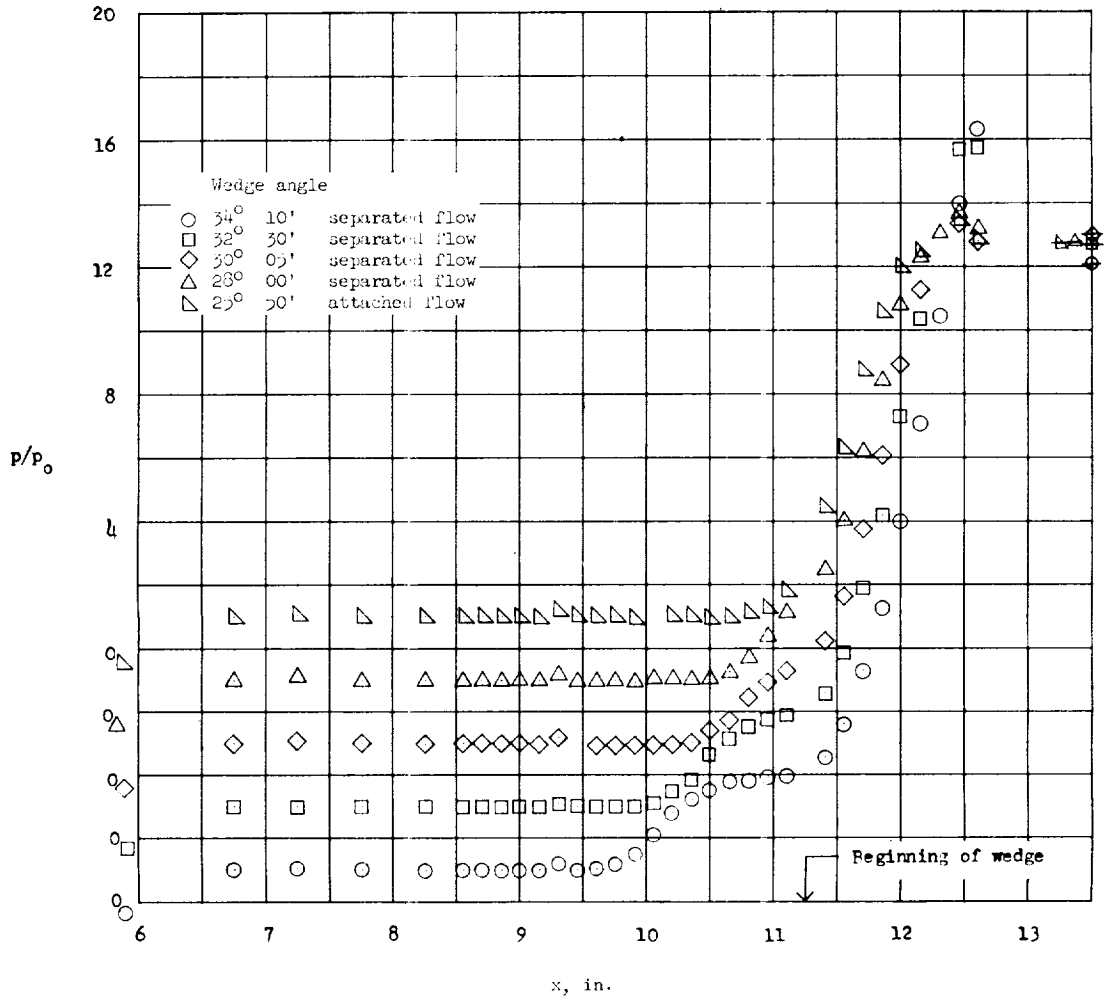

(b) Model 11-W with roughness.

Figure 8.- Continued.

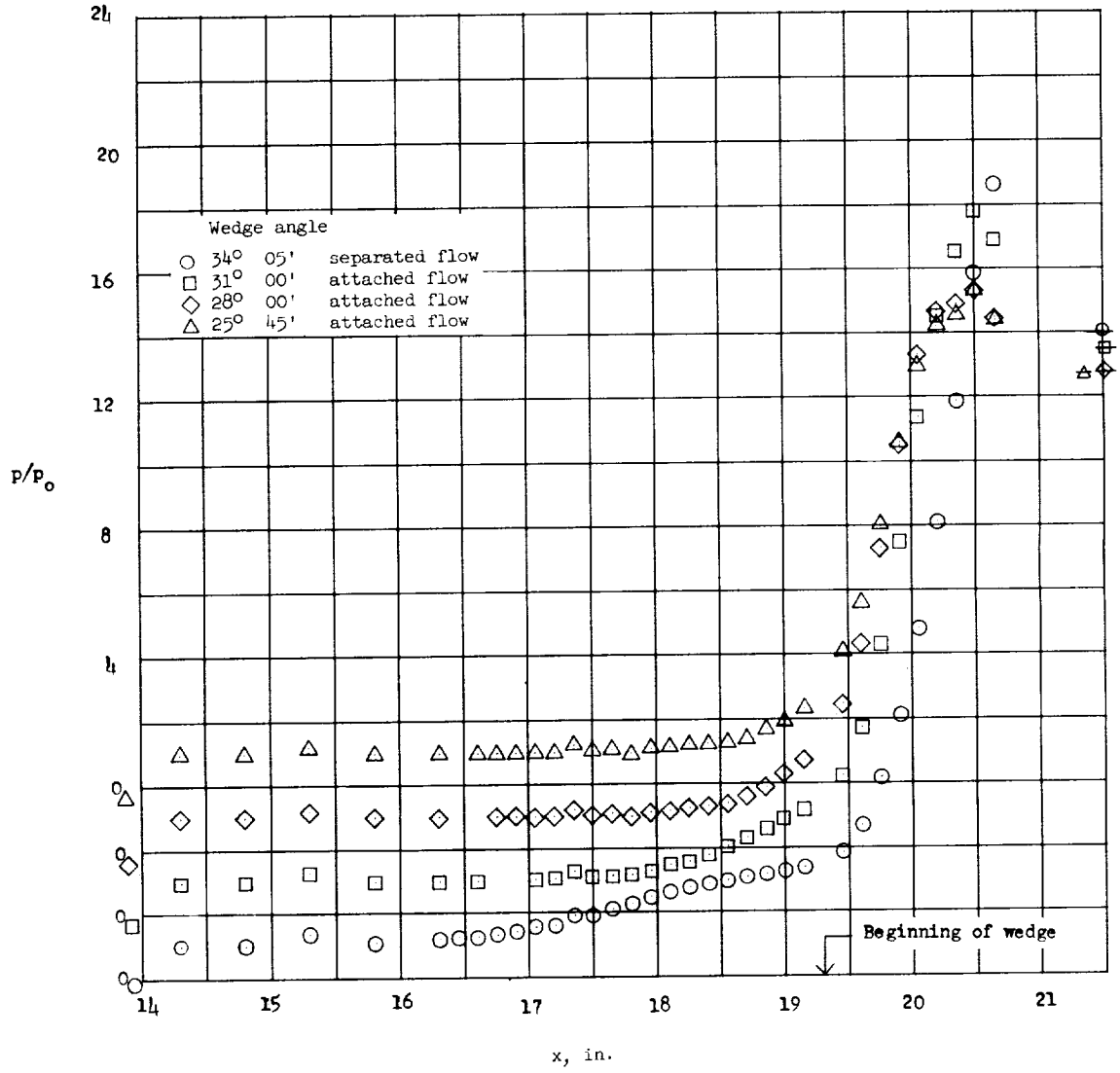

(c) Model 19-W without roughness.

Figure 8.- Concluded.

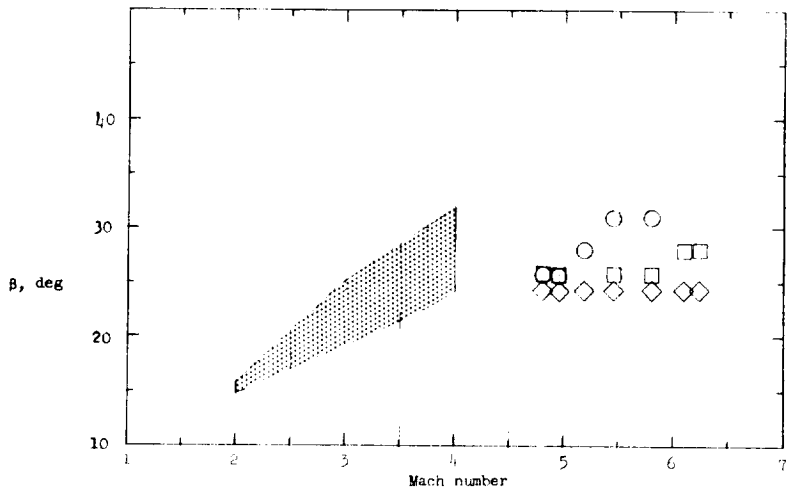

(a) Maximum wedge angle.

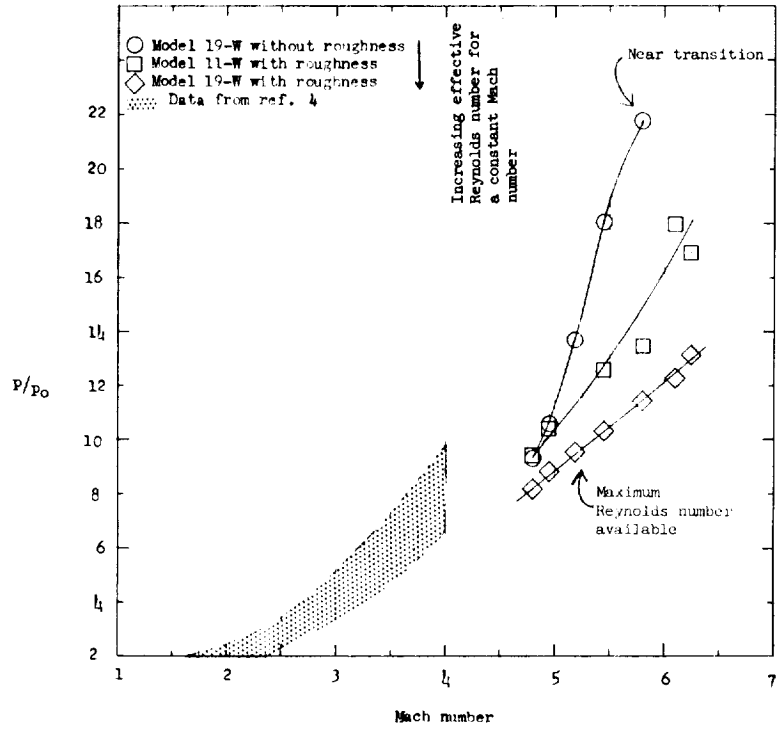

(b) Maximum pressure ratio.

Figure 9.- Maximum parameters for attached flow observed on wedges with different effective Reynolds numbers. p_t = 365 lb/sq in. abs.

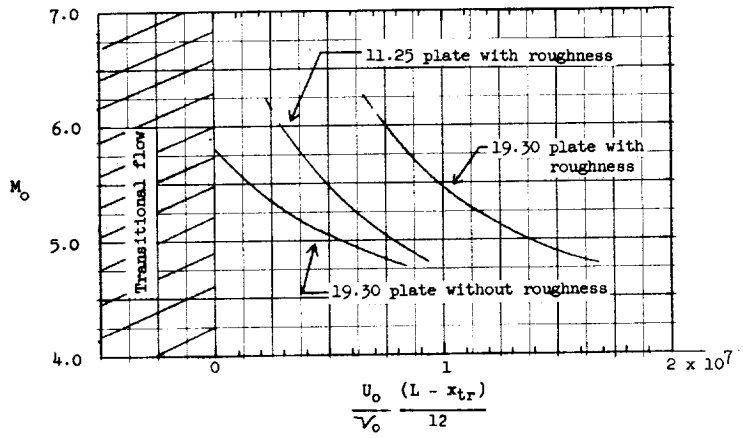

(a) Effective Reynolds numbers of basic plate as a function of Mach numbers.

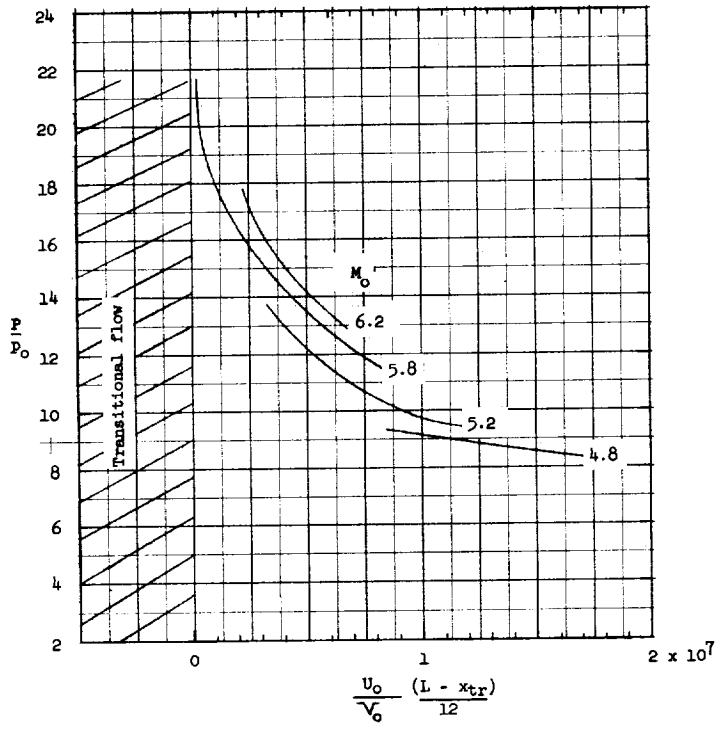

(b) Maximum pressure ratio for attached flow on wedges.

Figure 10.- Parameters as a function of effective Reynolds numbers R_e.

p_t = 365 lb/sq in. abs; $R_e = \frac{U_o}{\nu_o} \frac{(L - x_{tr})}{12}$.

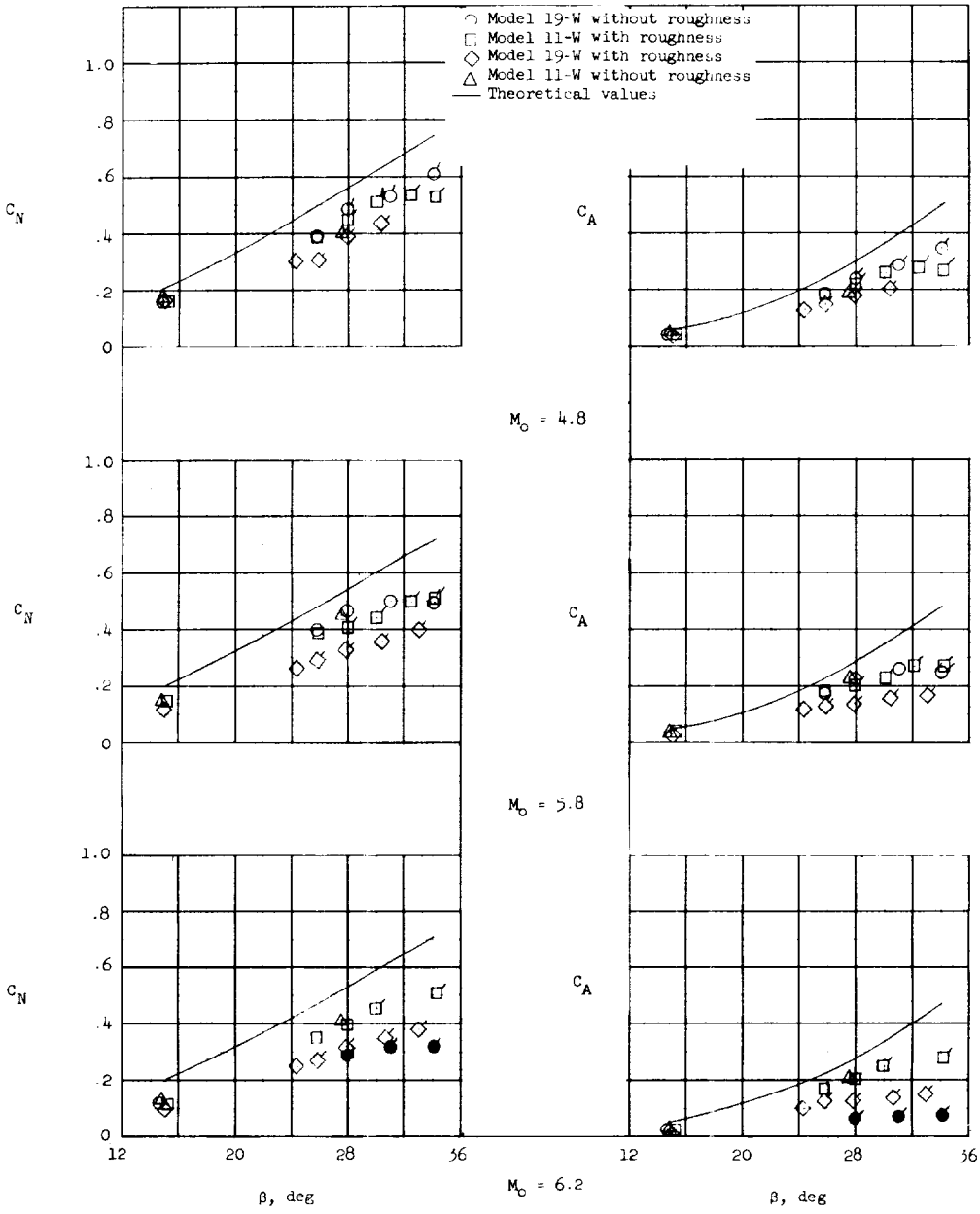

(a) Normal forces. (b) Axial forces.

Figure 11.- Comparison of normal and axial forces for different wedge angles with different effective Reynolds numbers. p_t = 365 lb/sq in. abs. Solid symbols are for transitional separation; flagged symbols are for flows with a separated region.

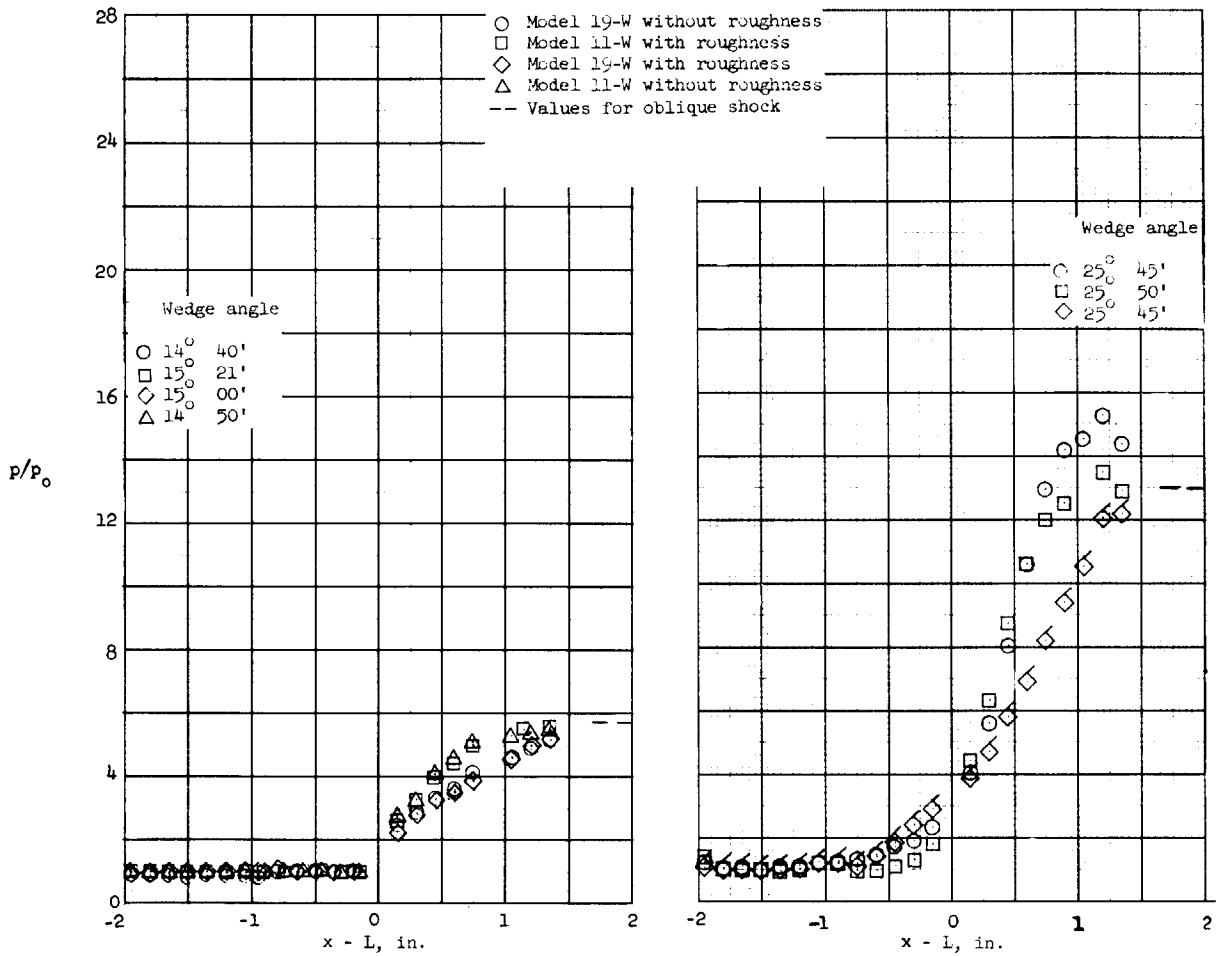

(a) Wedge angle ≈ 15°. (b) Wedge angle ≈ 26°.

Figure 12.- Pressure distributions observed on wedges at different effective Reynolds numbers. p_t = 365 lb/sq in. abs.; M_o = 5.8. Flagged symbols denote flow with a separated region.

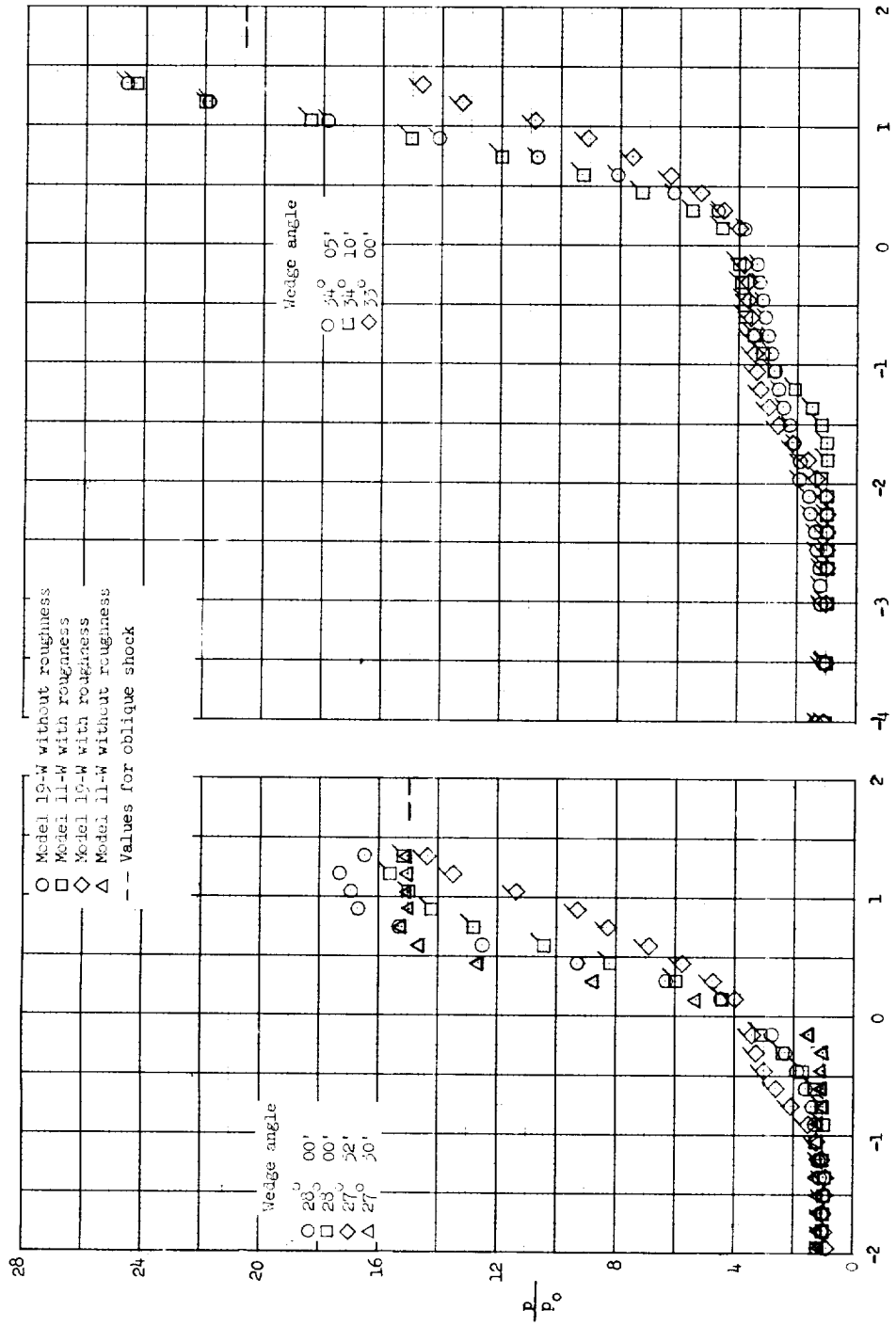

(c) Wedge angle ≈ 28°.

(d) Wedge angle ≈ 34°.

Figure 12.- Concluded.

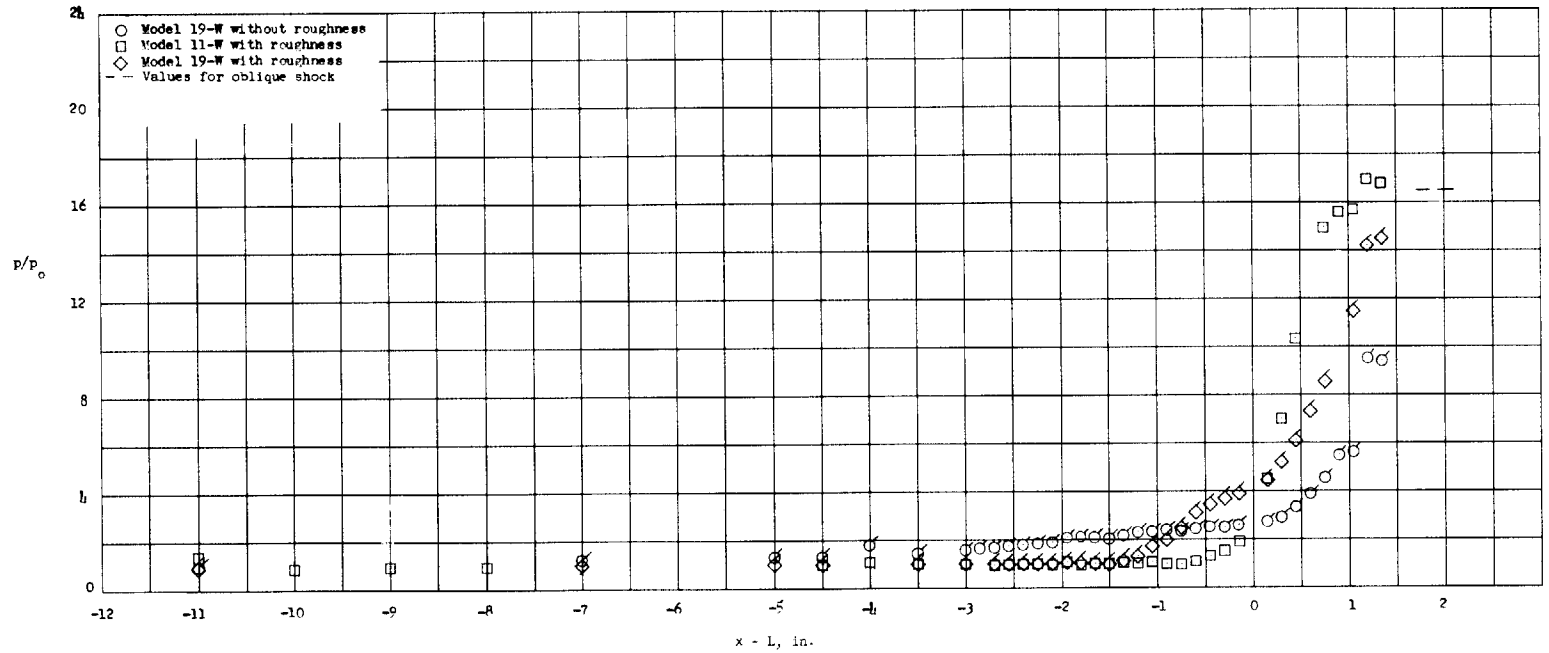

Figure 13.- Pressure distributions observed on wedges at different effective Reynolds numbers. p_t = 365 lb/sq in. abs.; M_o = 6.2; wedge angle ≈ 28°. Flagged symbols denote flow with a separated region.

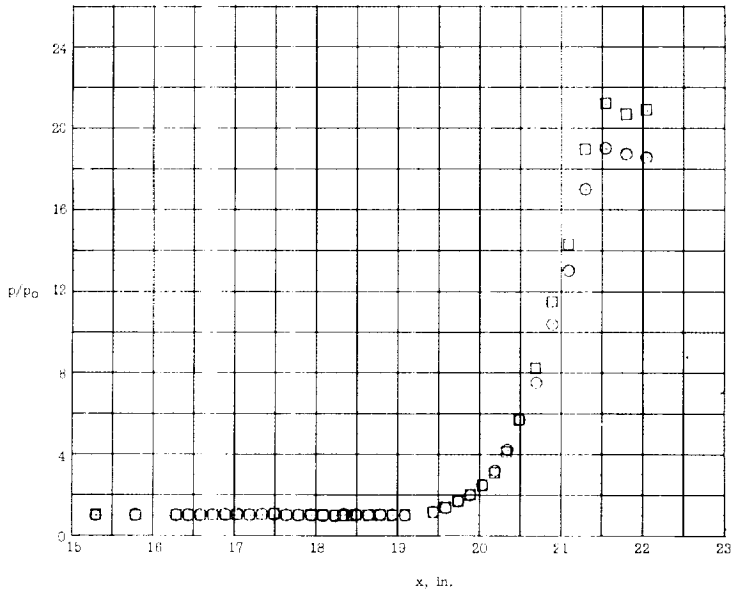

(a) $M_0 = 4.8$.

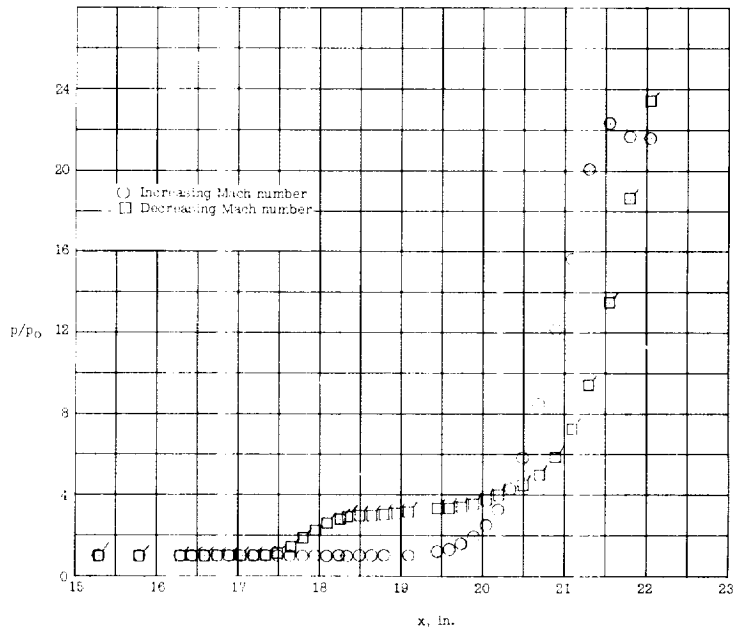

(b) $M_0 = 4.95$.

Figure 14.- Illustration of hysteresis effect on separation for model 19-C-4040-3.25 with roughness on plate. Flagged symbols denote separated flow.

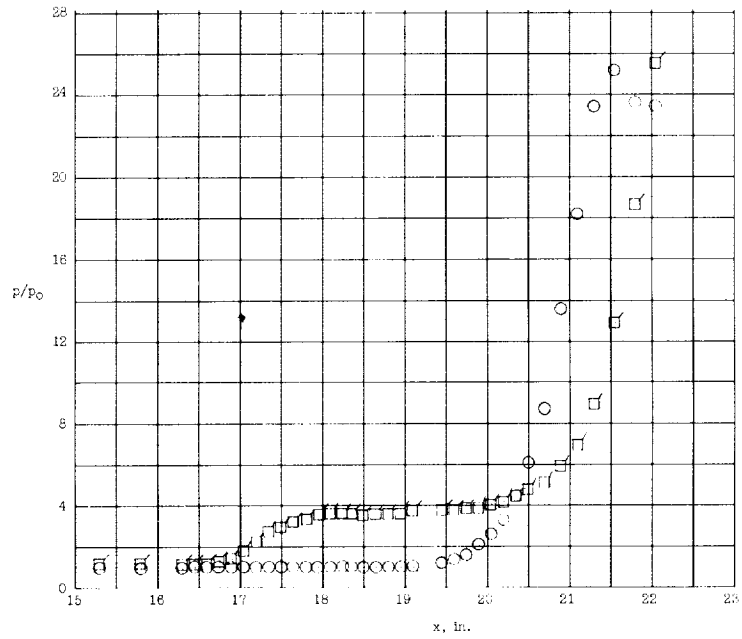

(c) $M_o = 5.45$.

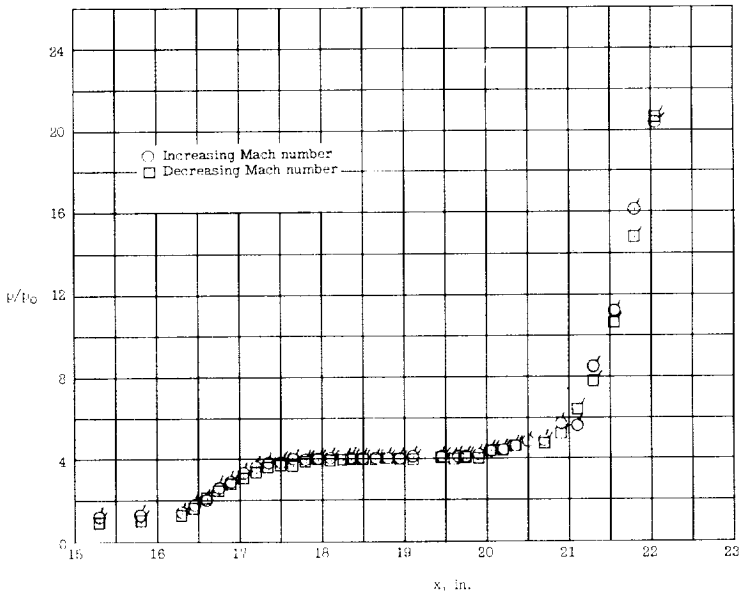

(d) $M_o = 5.8$.

Figure 14.- Concluded.

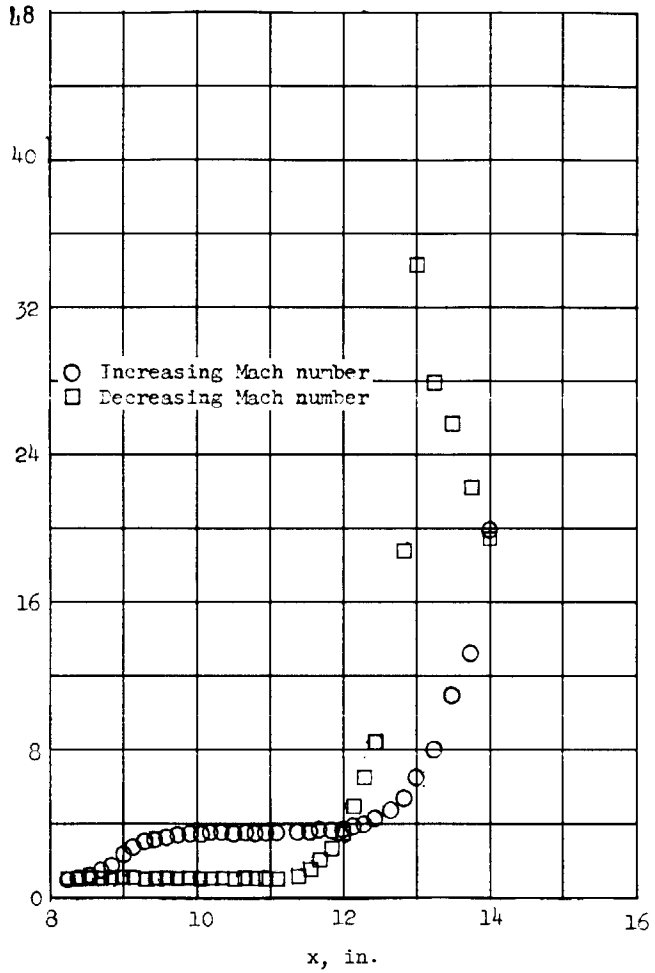

(a) Pressure distributions.

(b) Separation, increasing Mach number.

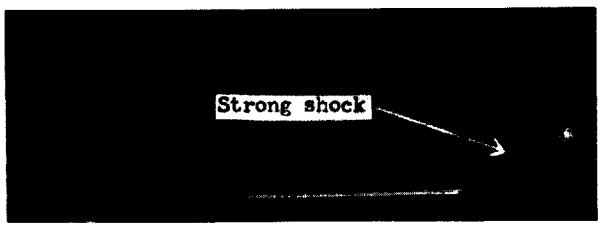

(c) Attached flow, decreasing Mach number.

L-61-7734

Figure 15.- Illustrations of hysteresis effect on separation for model 11-C-4042-3.25 with a smooth plate at $M_o = 4.8$.

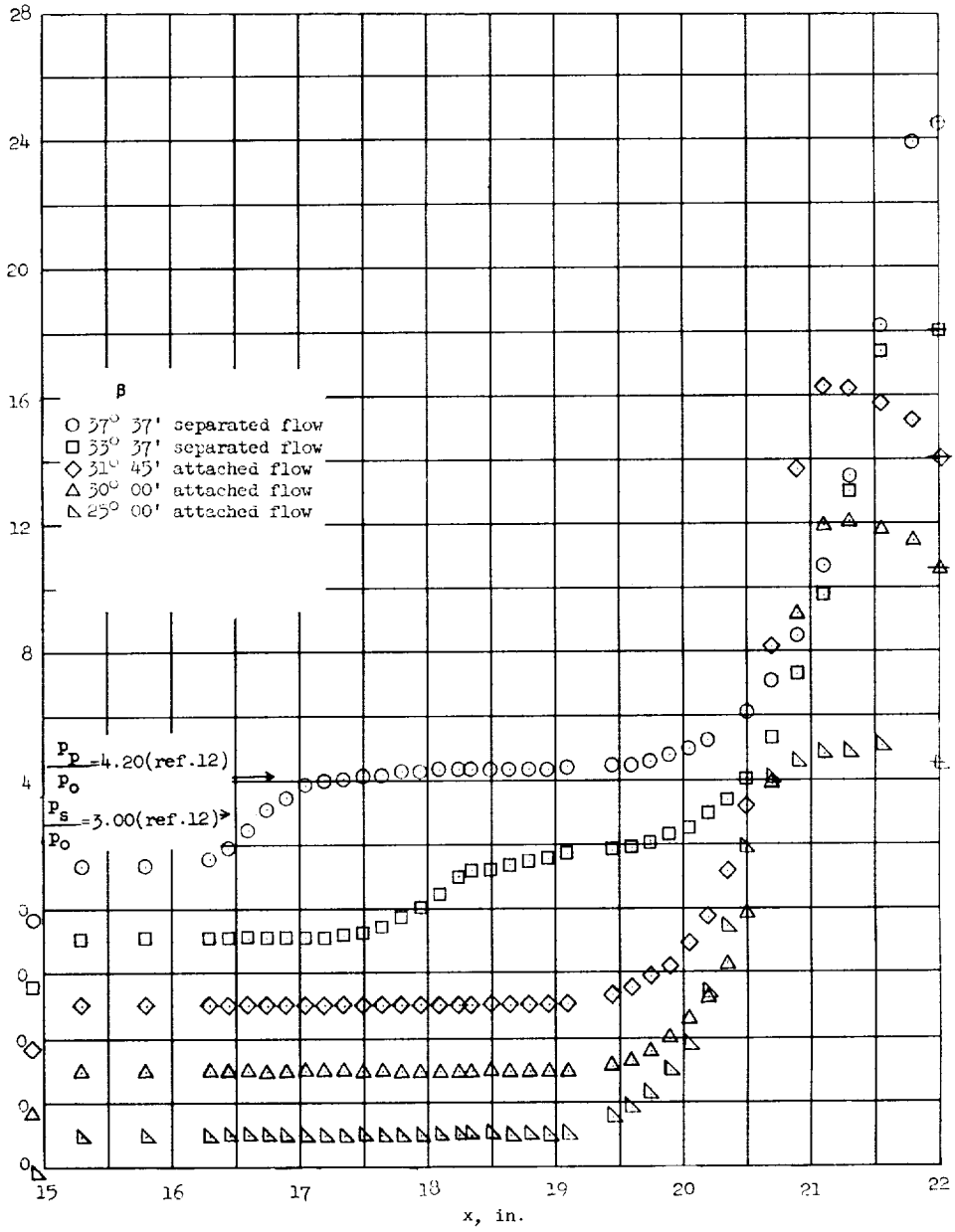

(a) 19.3-inch plate with roughness; 3.25-inch radius.

Figure 16.- Pressure distributions illustrating the occurrence of separation with an increase of surface angle for different effective Reynolds numbers at $M_o = 5.8$. Data taken when going from attached condition to separated condition. Bars through symbols denote theoretical oblique shock pressures.

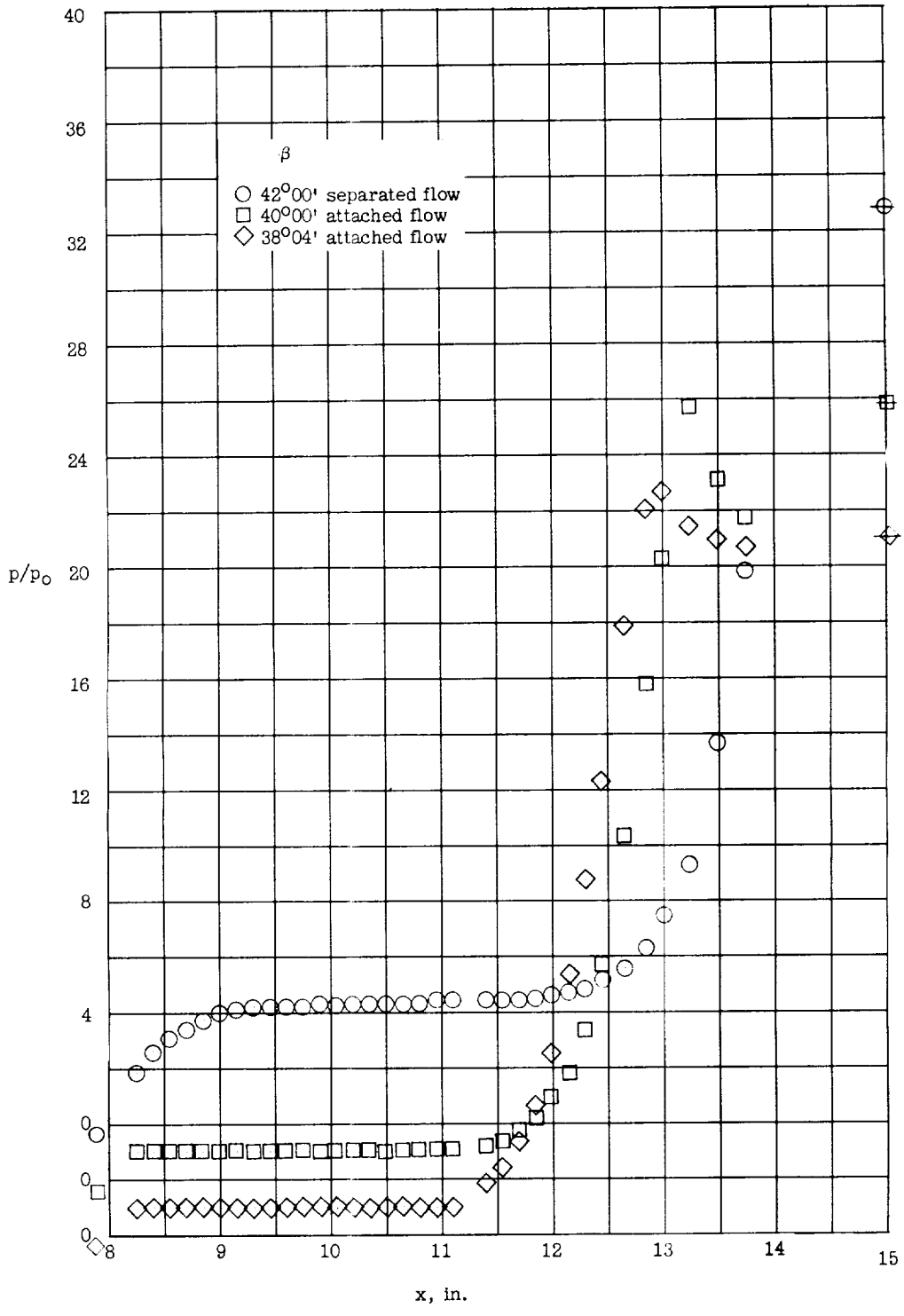

(b) 11.25-inch plate with roughness; 3.25-inch radius.

Figure 16.- Continued.

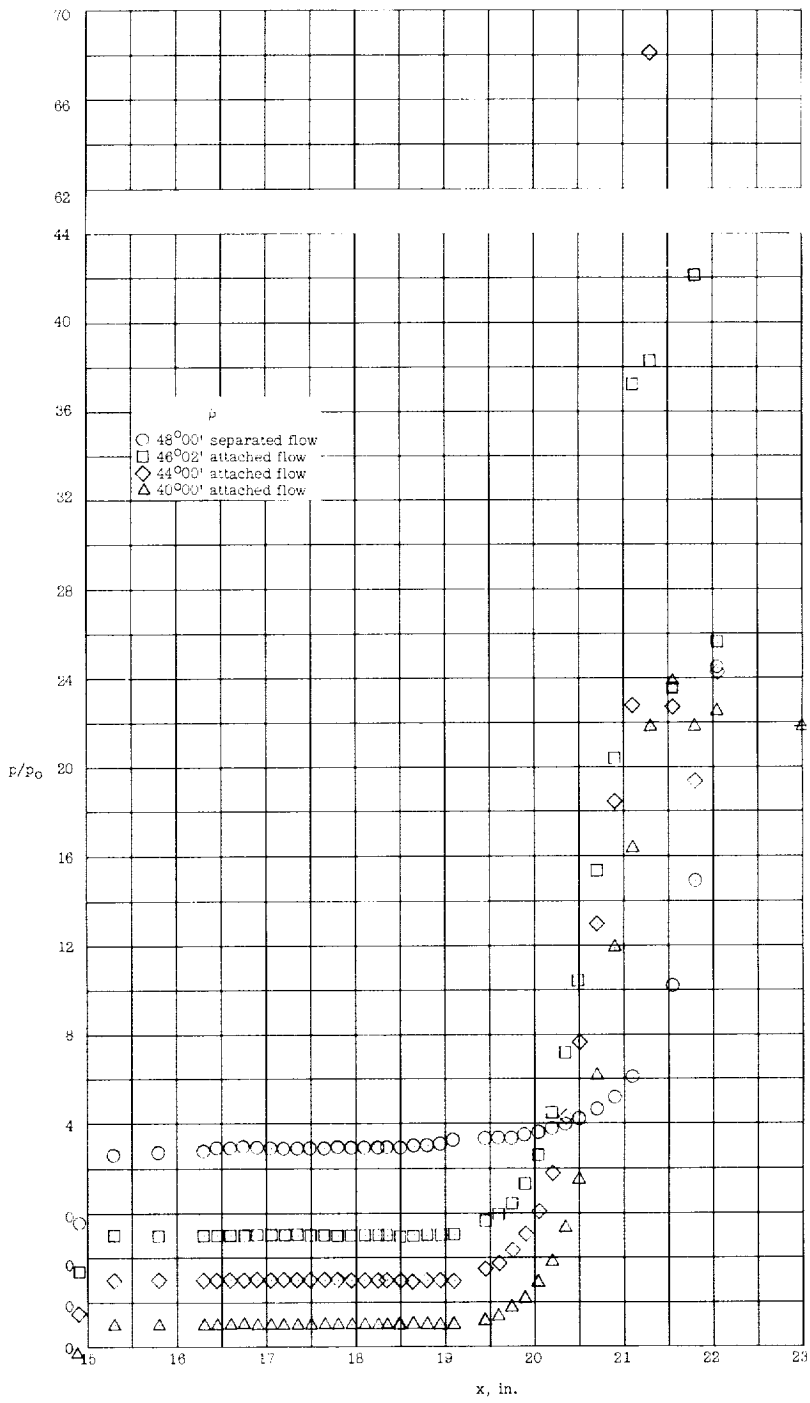

(c) 19.3-inch plate without roughness; 3.25-inch radius.

Figure 16.- Continued.

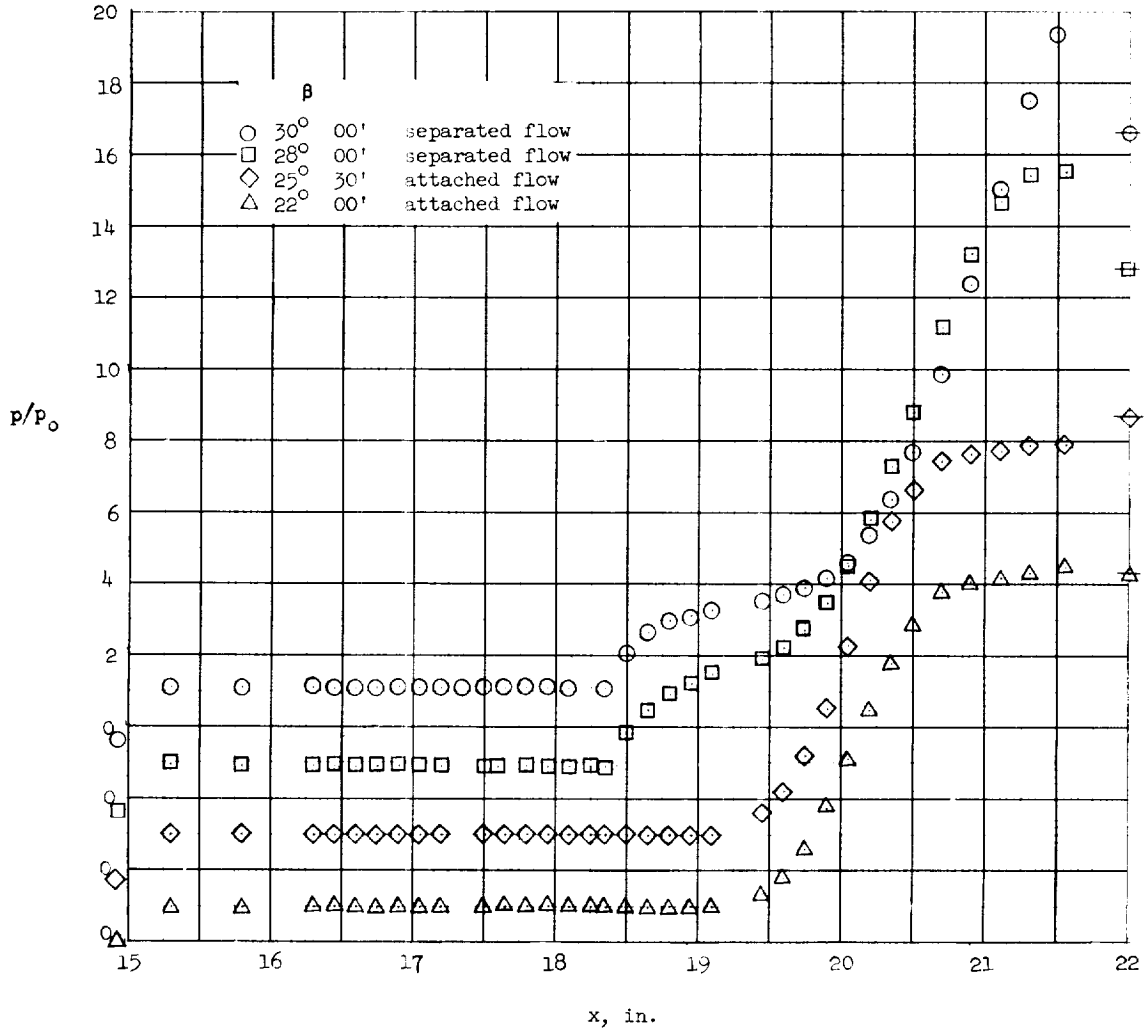

(d) 19.3-inch plate with roughness; 2.00-inch radius.

Figure 16.- Continued.

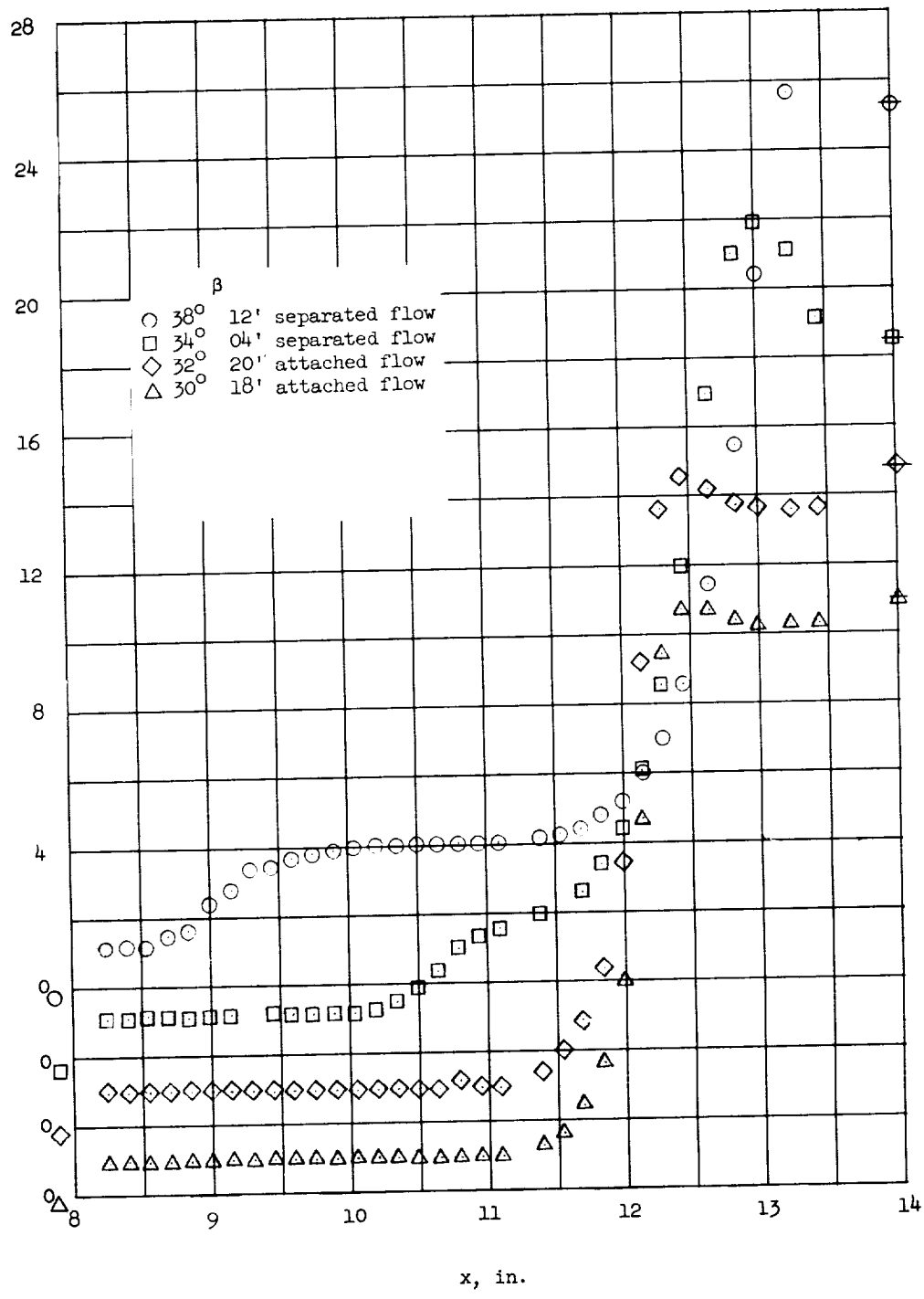

(e) 11.25-inch plate with roughness; 2.00-inch radius.

Figure 16.- Concluded.

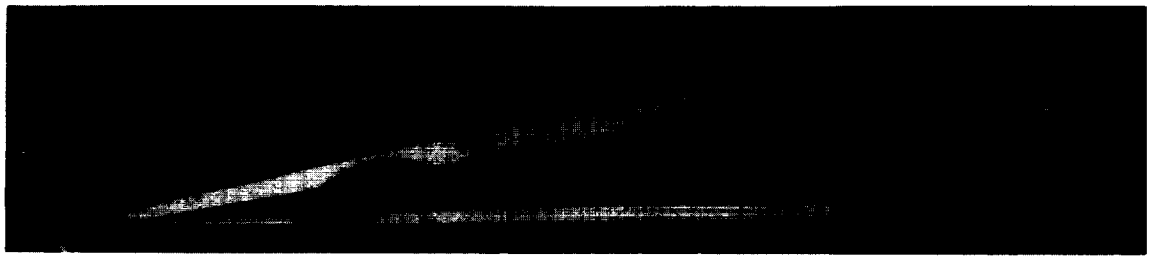

(a) Attached flow; $\beta = 38^{\circ}04'$.

(b) Attached flow; $\beta = 40^{\circ}00'$.

(c) Separated flow; $\beta = 42^{\circ}00'$. L-61-7735

Figure 17.- Schlieren photographs of flow over 3.25-inch curved surfaces on 11.25-inch plate with roughness. $M_o = 5.8$.

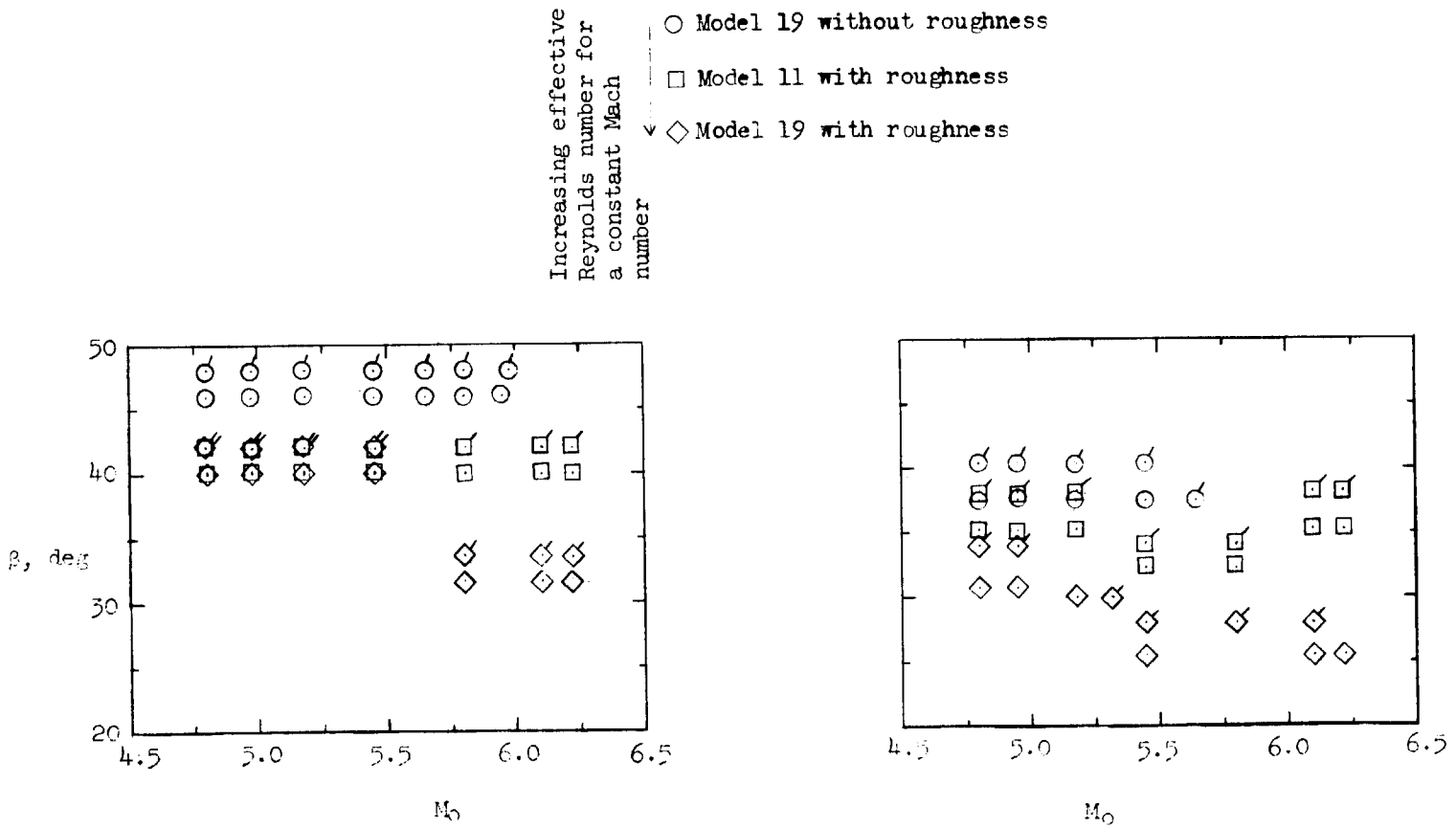

(a) 3.25-inch radius.

(b) 2.00-inch radius.

Figure 18.- Maximum angle with attached flow and smallest angle with separation for various effective Reynolds numbers. Data taken when going from attached condition toward separated flow condition. Flagged symbols denote data for separated flow condition; plain symbols, attached flow condition.

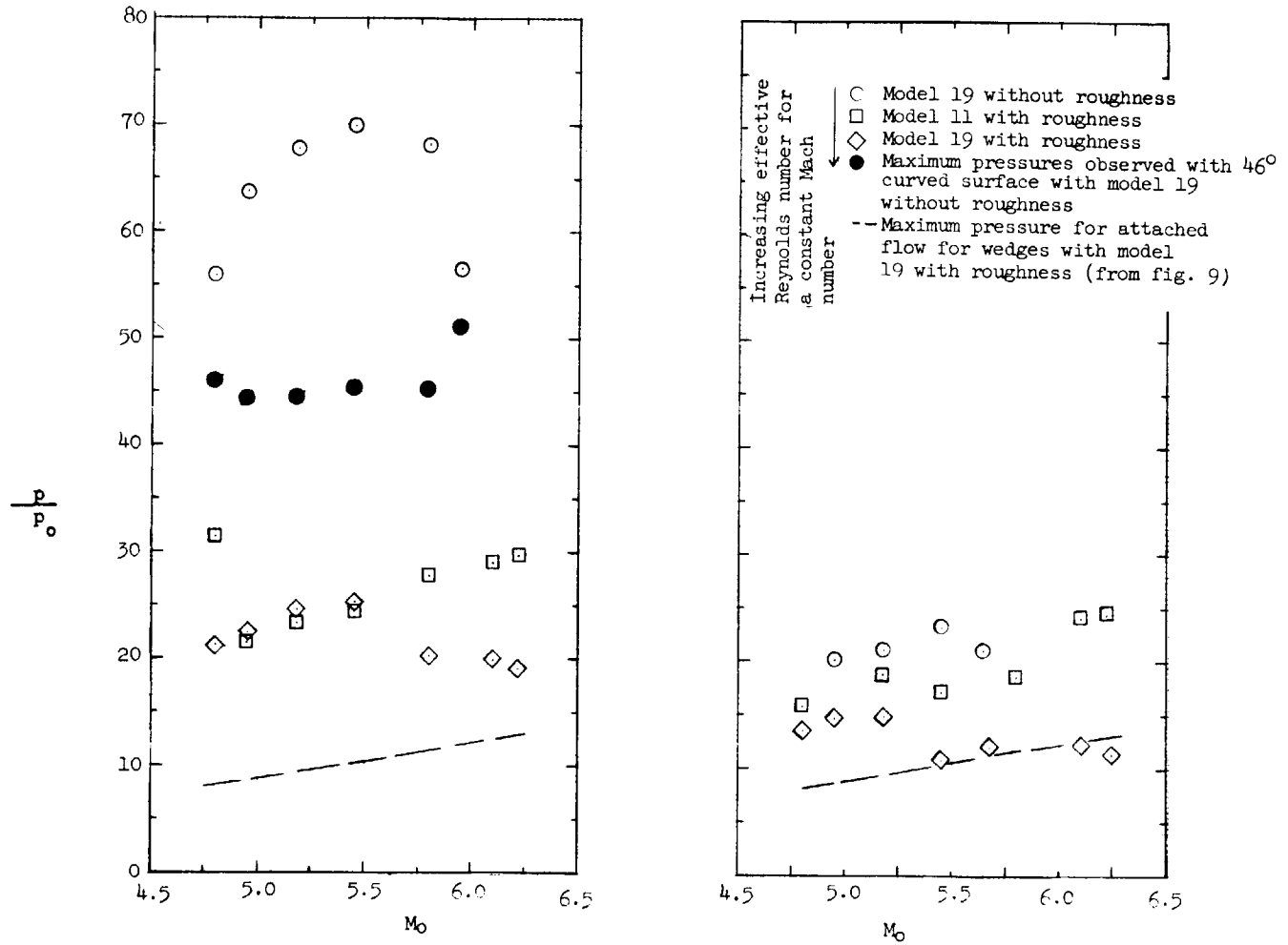

(a) 3.25-inch radius.

(b) 2.00-inch radius.

Figure 19.- Maxiumum pressure ratios for attached flow with various effective Reynolds numbers. Data taken when going from attached flow condition toward separated flow condition.

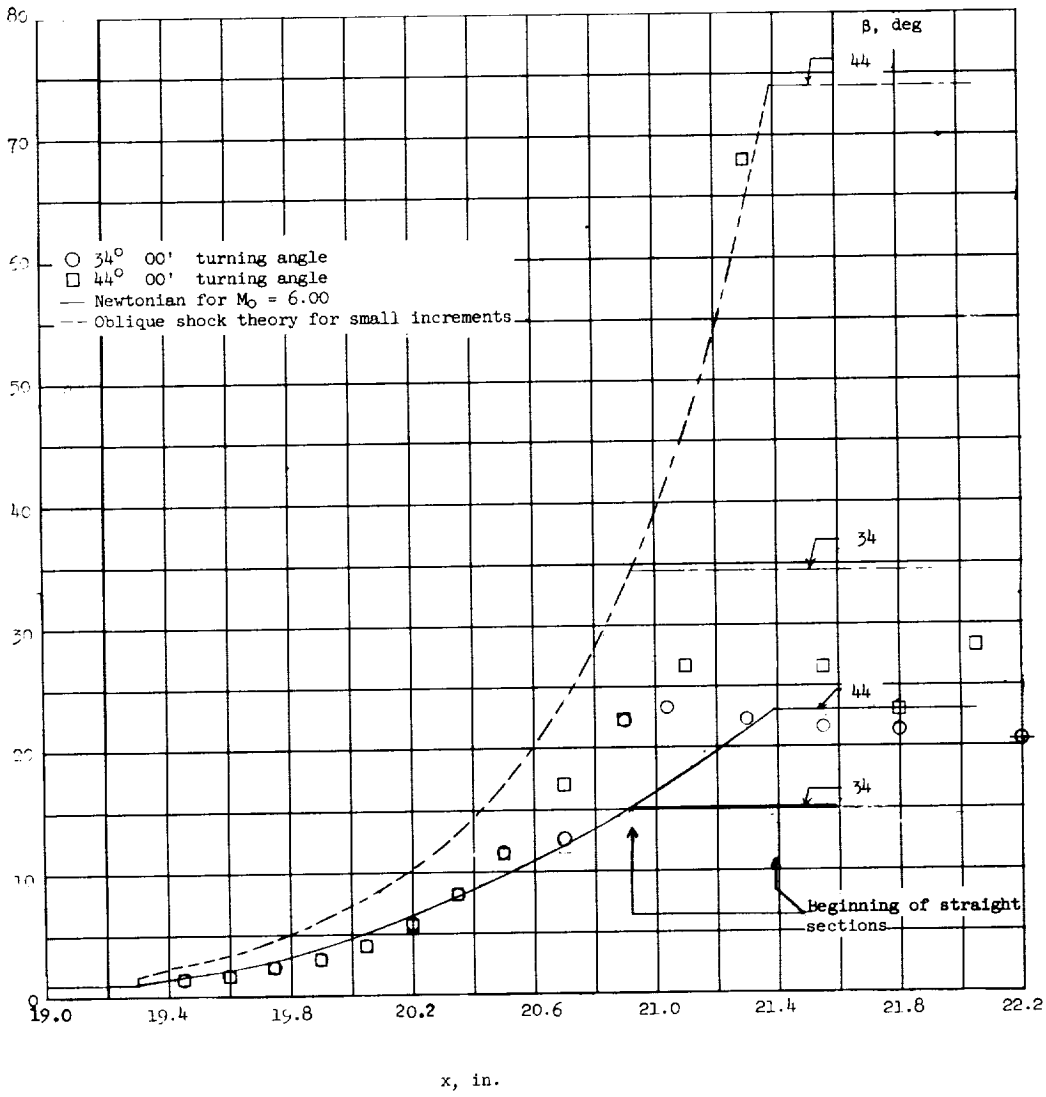

Figure 20.- A comparison of theoretical and experimental pressure ratios at M_o = 5.8. 3.25-inch radius models on smooth 19.3-inch plate. Bars through symbols denote theoretical oblique shock pressures.

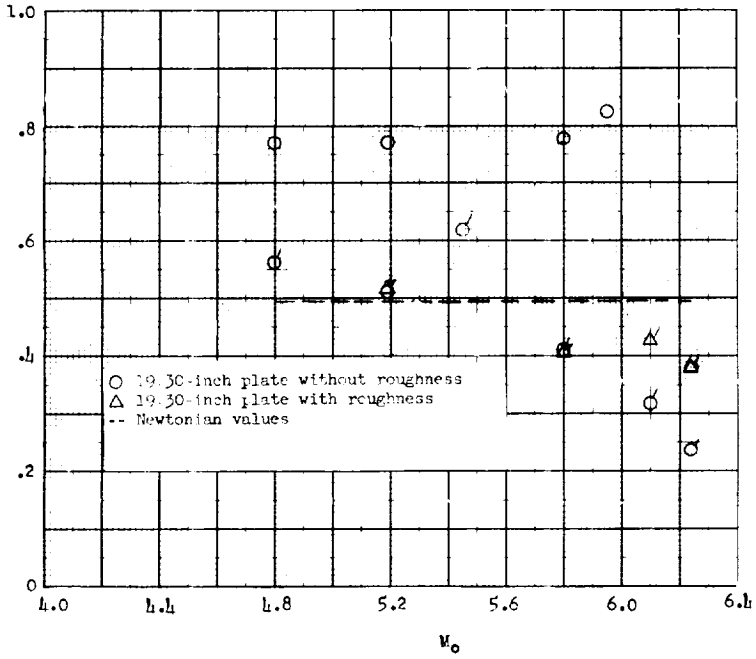

(a) $\beta = 46^{\circ}02'$.

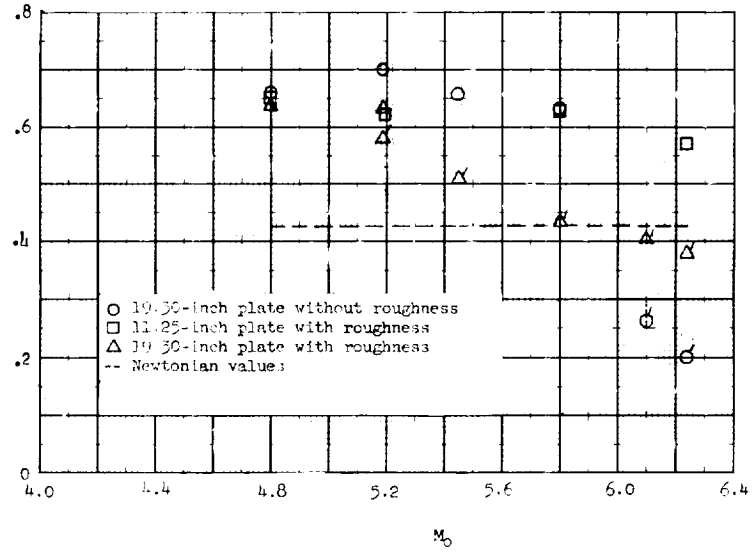

(b) $\beta \approx 38^{\circ}00'$.

Figure 21.- Normal-force coefficient values with and without separation at different effective Reynolds numbers. Flagged symbols denote separated flow.

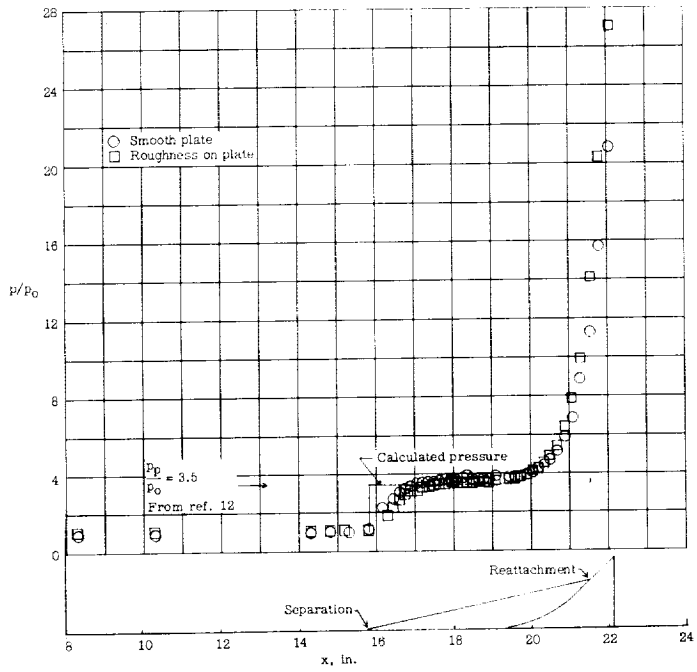

(a) M_o = 4.95; model 19-C-4046-3.25.

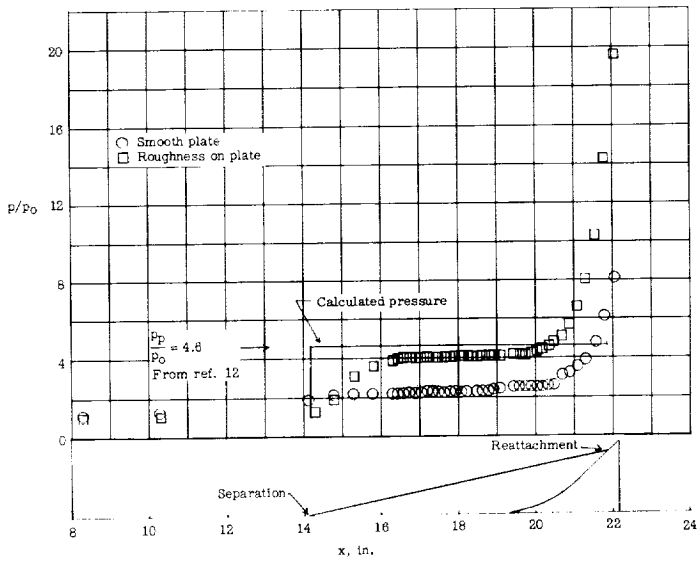

(b) M_o = 6.24; model 19-C-4046-3.25.

Figure 22.- Pressure distributions for separated flow with different effective Reynolds numbers for models on the 19.3-inch plate.

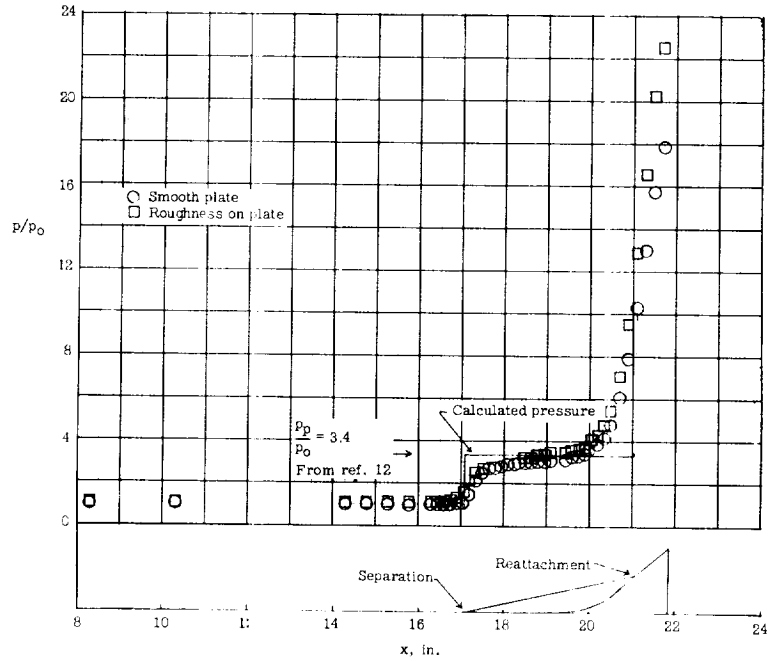

(c) M_o = 4.8; model 19-C-4040-2.00.

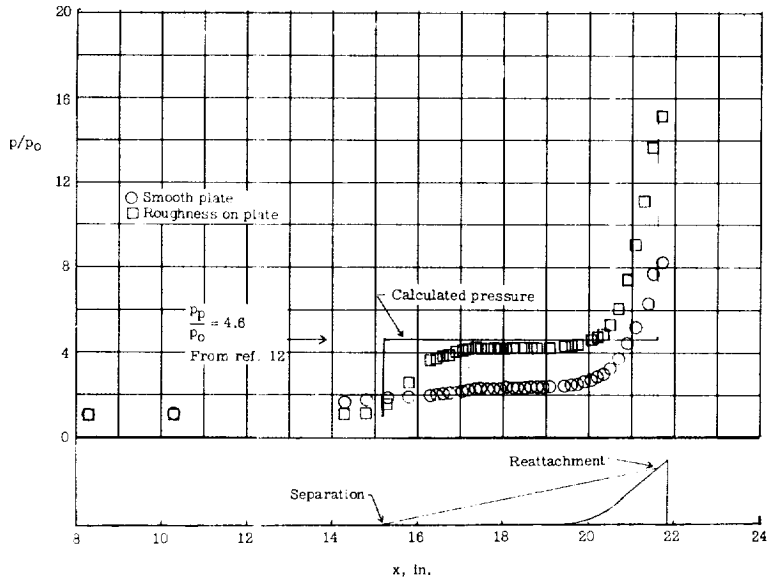

(d) M_o = 6.25; model 19-C-4040-2.00.

Figure 22.- Concluded.

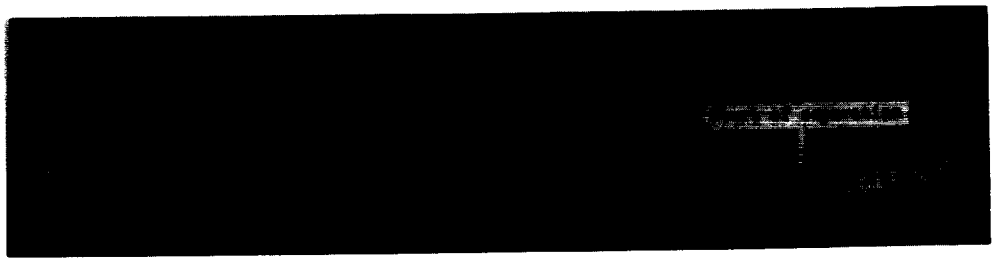

Smooth plate

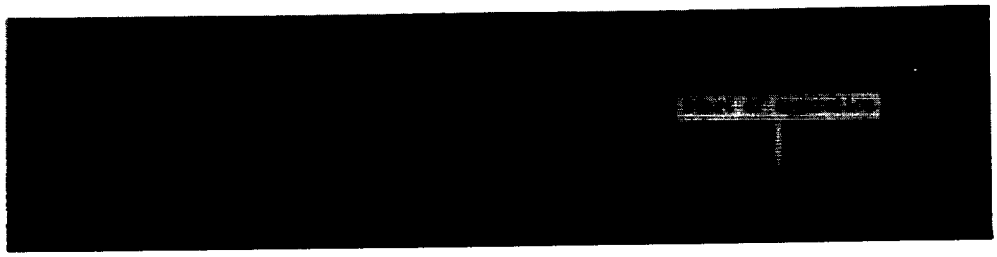

Roughness on plate

(a) M_o = 4.8.

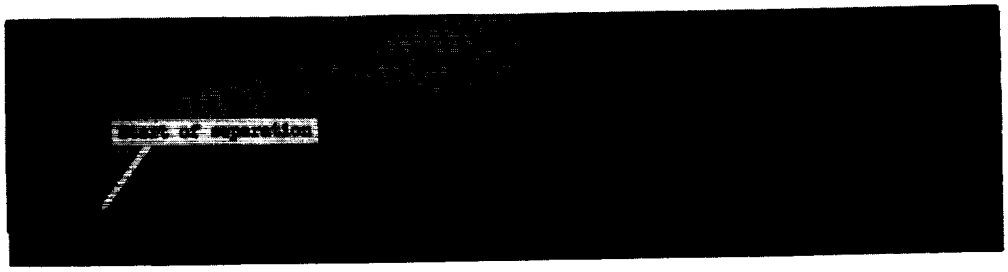

Smooth plate; transitional separation

Roughness on plate

(b) M_o = 6.24. L-61-7736

Figure 23.- Schlieren photographs showing flow separation over model 19-C-4040-2.00 with different effective Reynolds number at two Mach numbers.

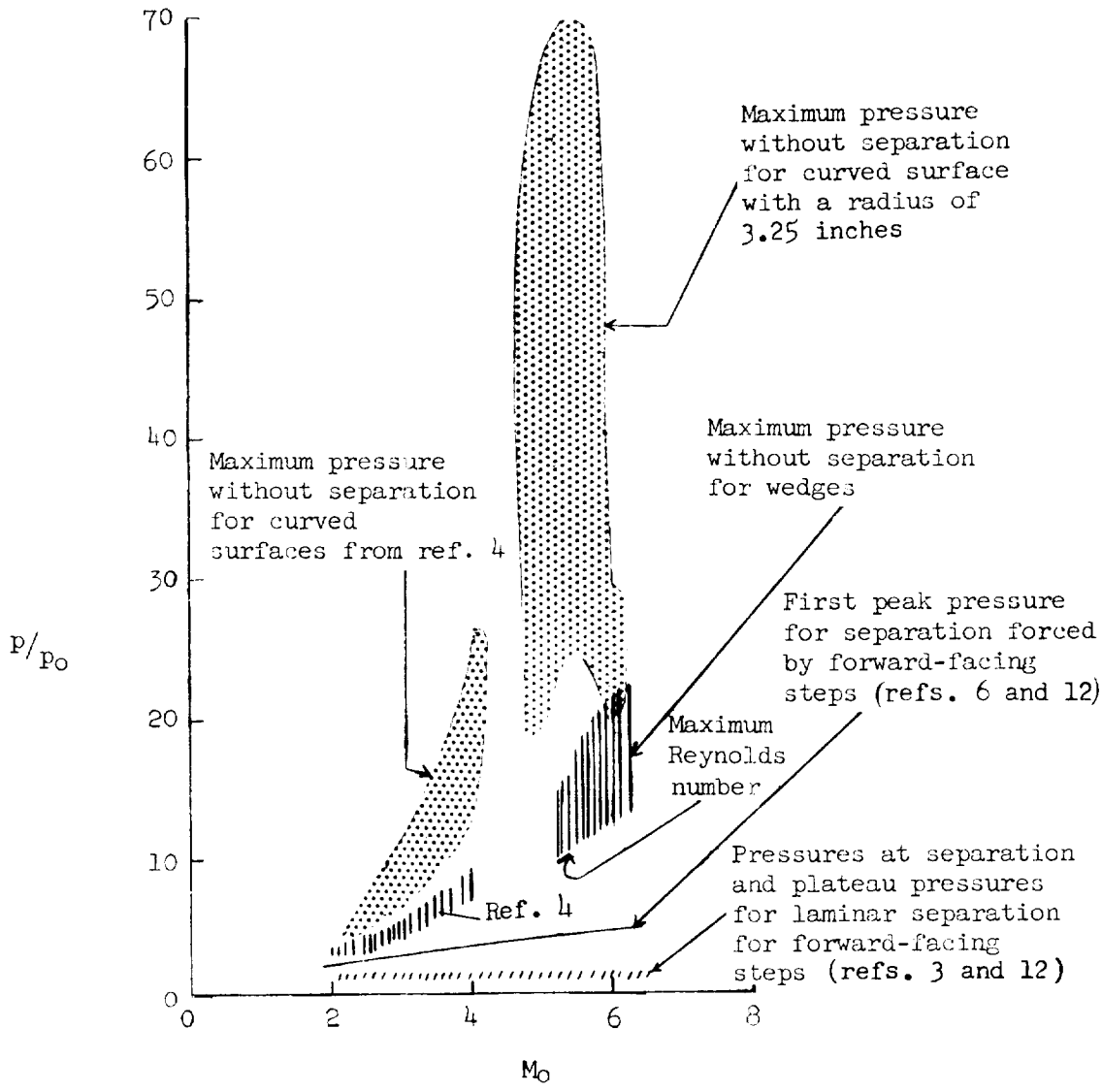

Figure 24.- Summary curves for two-dimensional turbulent separation.